Delft University of Technology

Automatic Flight Control System Design Practicum
AE4301P

Design of some autopilot systems for the Lockheed Martin F-16 model

Authors:
Luc Kloosterman (4697006)
Barry van Leeuwen (4390792)
Prawien Kanhai (4615220)

February 21, 2020

Contents

Introduction

The goal of this project is to design a control system using classical control theory for the F16 military aircraft [1]. In this report only the pitch rate command system and the glideslope following and flare controller will be covered. At the base of this practicum stands the non-liner F16 model from professor G.J. Balas from the University of Minnesota. It simulates the response of an actual F16 using one of two models specified as the low fidelity and high fidelity model. During this report only the low fidelity report will be used.

Before any control system can be designed the aircraft model will be trimmed and linearised and the influence of the accelerometer position will be analysed in the first section. After this, an open loop analysis of the longitudinal and lateral motions will be carried out. From this analyses a pitch rate command system can be designed. Finally, an automatic glideslope following and flare controller will be designed. Throughout the report different flight conditions will be used to linearise the F-16 model. Table 1 summarises these flight conditions.

Section	**Altitude [ft]**	**Velocity [ft/s]**
Chosen Flight Condition	30000	600
Accelerometer Position Analyses	15000	500
Automatic Glideslope and Flare Mode	5000	300

Table 1: Flight condition throughout the report

1 Trim and Linearisation

In order to obtain a meaningful linearised result it is absolutely necessary to do a trim procedure first. By trimming the aircraft an equilibrium point will be defined around which the aircraft can be linearised. The LTI system will not represent the chosen flight condition if the operating point is not around an equilibrium. For trimming and linearising the aircraft a Steady Wings-Level Flight condition is chosen. The `FindF16Dynamics.m` file carries out the trim and linearisation for both the high and low fidelity model. From this the resulting longitudinal and lateral directional modes can be distracted. Furthermore, it finds the poles-zero mapping of the modes and the corresponding damping ratio and natural frequencies. In order to achieve the desired order of accuracy some iterations are needed. With every iteration the cost function will be minimized by varying the thrust and the different control surfaces until the derivatives have gone to zero. The accuracy will then be presented in terms of a cost value. *"Values on the order of 10e-29 and 10e-6 are common for the low and high fidelity model"*[2]. From table 2 it can be seen that a second iteration is only needed for the flight condition at 30000 ft and 600 ft/s for the high fidelity model.

Flight Condition [ft, ft/s]	**15000 ft, 500 ft/s**		**30000 ft, 600 ft/s**	
Iterations	**High Fidelity**	**Low Fidelity**	**High Fidelity**	**Low Fidelity**
1	7.1856e-06	2.2909e-29	1.2129e-04	2.6836e-29
2	7.1856e-06	2.2907e-29	4.5276e-06	3.163e-30

Table 2: Cost values in the high and low fidelity model at different flight conditions

1.1 Influence of the Accelerometer Position Analysis

In this section the normal acceleration (a_n) position will be analysed and added to the F-16 model. In order to do this the formula for (a_n) ,which is given by equation 1, has to be added to the `LIN_F16block.mdl`. To successfully do this the states 11 and 15, which are $\dot{q}$ and n_z respectively, have to be extracted from the signal coming out of the c-block as shown in figure 1. The constant c is defined in the model as $\frac{x_a}{g_d}$ where the gravitational acceleration g_d is $32.1737 ft/s^2$ and the accelerometer position x_a is positive in the X_{body} axis.

$$a_n = n_z + \frac{\dot{q} x_a}{g_D} \tag{1}$$

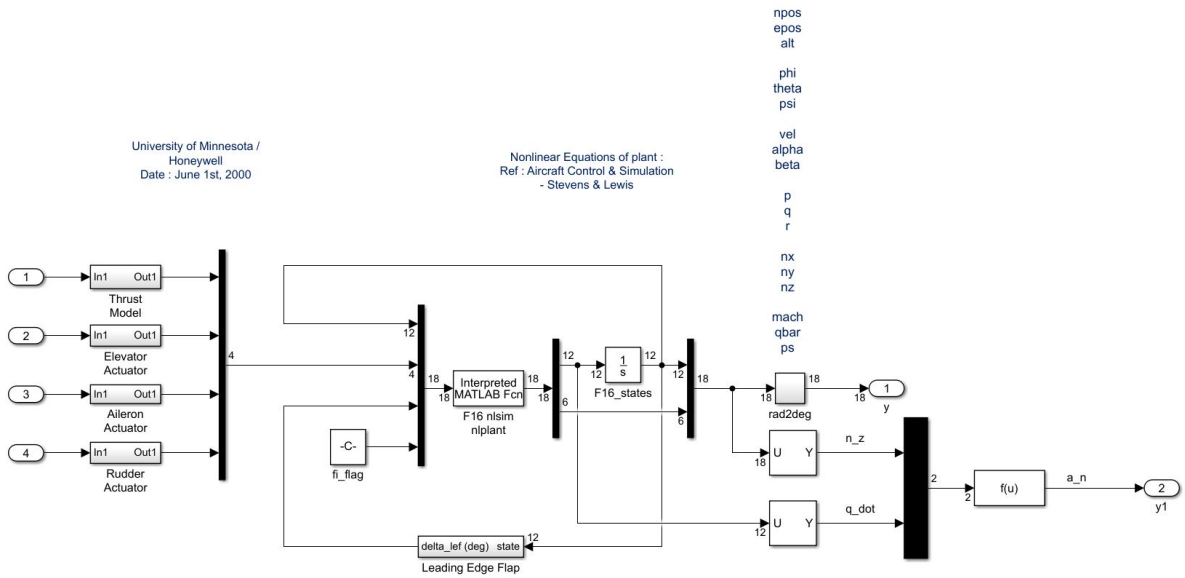

Figure 1: Simulink model with the normal acceleration added

The result of adding the normal acceleration is a 19th row in the output matrix, $y = C\bar{x} + D\bar{u}$, which is the additional output a_n. With this addition the state equation, $\dot{\bar{x}} = A\bar{x} + B\bar{u}$, is not changed. The linearized output equation 2 of a_n when the accelerometer is placed at the centre of gravity ($a_n = 0$) is expected to be the same as n_z.

$$a_n = -3.2432 \cdot 10^{-5}h - 9.6796 \cdot 10^{-6}\theta + 0.0040v + 9.1988\alpha + 0.5566q - 0.0321\delta_e \tag{2}$$

The remaining states of matrices C and D are zero for a_n and are therefore not listed in the equation. The normal acceleration is depend on the altitude (h), pitch angle (θ), velocity (v), angle of attack (α), pitch rate (q) and the normal force (δ_e). The angle of attack is significantly the most dominant variable in the equation and the altitude and pitch angle are negligible. A different elevator-to-normal-acceleration transfer function can be found for different inputs on all flight conditions. Equation 3 shows the transfer function where the accelerometer is placed at the centre of gravity with a Steady Wings-Level Flight condition at an altitude of 15000 ft with a velocity of 500 ft/s.

$$\frac{a_n}{\delta_e} = \frac{0.421s^4 - 1.84s^3 - 22.15s^2 + 0.077s + 0.001231}{s^5 + 21.73s^4 + 33s^3 + 41.48s^2 + 0.5546s + 0.293} \tag{3}$$

In figure 2 the normal acceleration to a negative step elevator command is shown. In order to analyse the long time span and the initial response during the first few seconds the plot is divided in two subplots of the same time response. The top plot shows the response during the first three seconds and the lower plot shows the the smooth time response over 300 seconds.

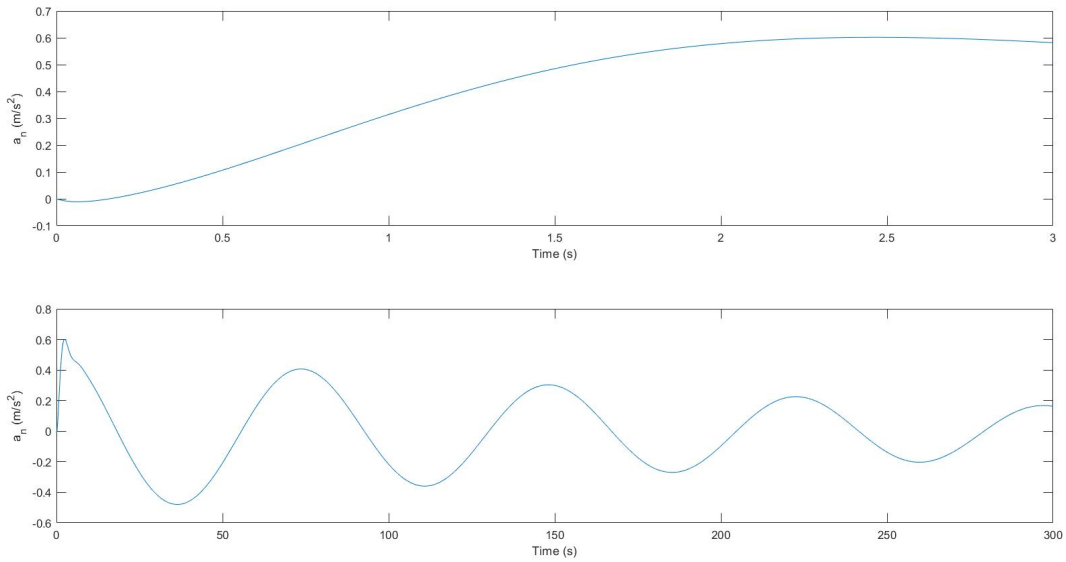

Figure 2: Normal acceleration to a negative step elevator command

In the top plot it can be seen that the initial response in the first 0.2 seconds is in the opposite direction of the reference signal. The cause of this behaviour can be found in the numerator of the transfer function. From the numerator the zero's of the system can be found by solving for s where the numerator is equal to zero. The zero's do not have any influence on the longer time span but a zero in the open right half plane is the cause for an initial response in the opposite direction. Figure 3 shows the root locus of the transfer function, it clearly can be seen that the zero responsible for this behavior is the one most to the right. This behavior is defined as non-minimum phase behavior.

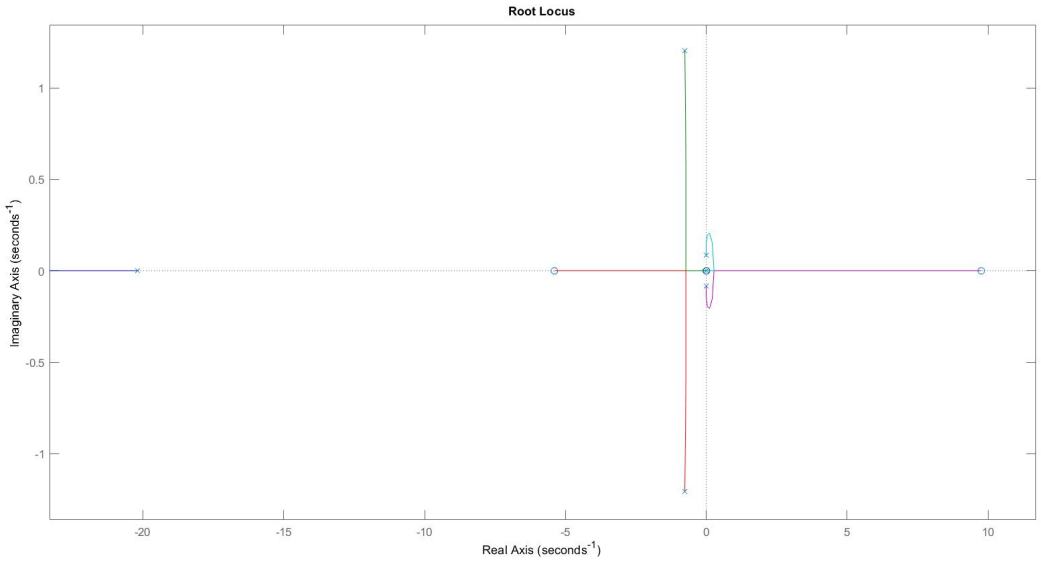

Figure 3: Root locus of elevator-to-normal-acceleration transfer function

When a negative step elevator command is executed the aircraft will first have a pitch up motion. Because of this motion the tail will experience a downwards acceleration first before accelerating upwards. This causes a direct reduction in lift which results in a slight drop which is experienced as negative acceleration. After this drop the aircraft will respond to the pitch motion and increase its lift resulting in a positive normal acceleration.

The transfer function zero values for accelerometer position $x_a = 0ft$, $x_a = 5ft$, $x_a = 5.9ft$, $x_a = 6ft$, $x_a = 7ft$ and $x_a = 15ft$ are shown in table 3. The initial time response is shown in figure 4 which shows that the non-minimum phase behavior only occurs at $x_a = 0$ and $x_a = 5$. When analysing the zero values for different accelerometer positions it can be seen that for $x_a = 0$ and $x_a = 5$ a positive zero exists which means it is located in the open right half plane of the root locus. For all other accelerometer position this zero is negative and therefore lies in the open left half plane. Zero's are more dominant when they are positioned close to a pole. In table 3 it can be seen that for $x_a = 5.9ft$ the zero lies at -67170 which is definitely far away from all poles in the root locus. Therefore, it is safe to conclude that the instantaneous centre of rotation has a negligible distance from $x_a = 5.9ft$ and the assumption can be made that this point is the instantaneous centre of rotation.

zero values for accelerometer positions [ft]					
$x_a = 0ft$	$x_a = 5ft$	$x_a = 5.9ft$	$x_a = 6ft$	$x_a = 7ft$	$x_a = 15ft$
9.7596	40.673	-67170.4	-283.72	-13.735 + 9.6727i	-1.9412 + 5.5105i
-5.3925	-8.4873	-10.519	-10.898	-13.735 - 9.6727i	-1.9412 - 5.5105i
0.0093895	0.0093883	0.0093881	0.0093881	0.0093878	0.0093859
-0.0059186	-0.0059185	-0.0059185	-0.0059185	-0.0059185	-0.0059183

Table 3: zero values for different accelerometer positions

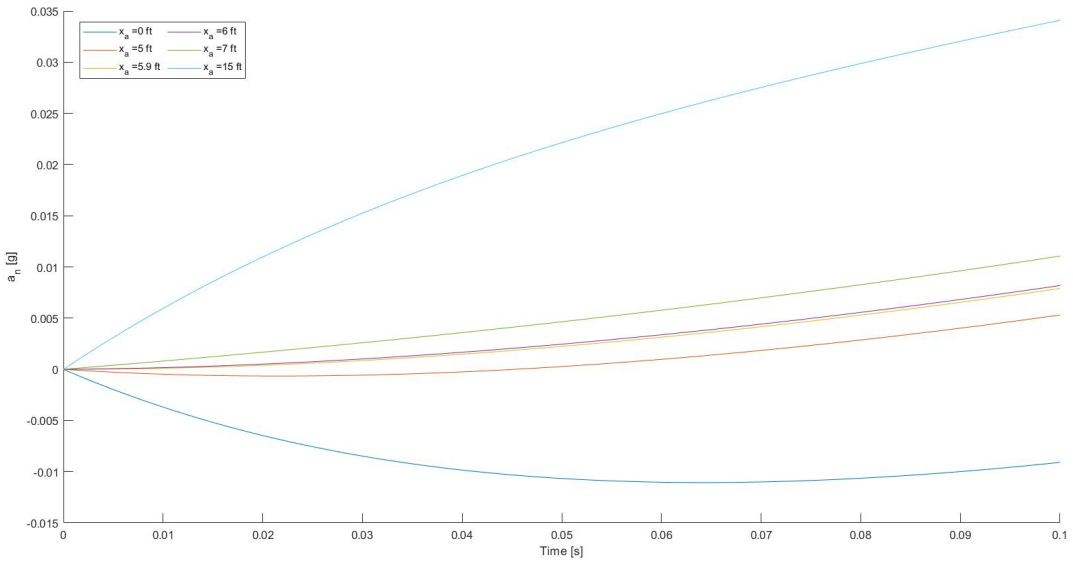

Figure 4: Initial time response for different accelerometer positions

The pilot station should preferably be located close to the centre of rotation. When the station is placed more to the front the pilot will experience a normal acceleration in the opposite directions as he will expect. The pilot will most likely compensate for this acceleration and try to reverse this response. On the other hand, if the station is placed far behind the centre of rotation the pilot will experience a higher g-force. This is unwanted because it is uncomfortable for the pilot and can result in a black out more easily.

The position on the aircraft at which the bending loading is the highest is called the most important fuselage bending mode. For safety it is important that the accelerometer is placed close to this point. If this is not done, structural oscillations will be coupled into the rigid-body control system and may degrade the handling qualities or even lead to an “aeroservoelastic” limit cycle oscillation [3].

2 Open Loop Analysis

In this section the LTI state space models of the longitudinal and lateral motions are computed from the F16 model. The open loop analysis is about the situations where there are no control or stability augmentations added to the aircraft model. In this open loop analysis first the LTI state space model matrices will be computed. After this, an analysis regarding the eigenmotions and their characteristics will be carried out. Finally, the time responses of the eigenmotions will be analysed.

2.1 LTI state space model computations

The open loop behavior of the F16 model can be represented by the LTI state space model. This LTI state space model is represented by a simplified low fidelity trimmed model at 3000 ft and 500 ft/s. This model for longitudinal motion is represented by equation 4 which consists of A and B matrices with V_t, α, θ, q and δ_{el} as the states and u_{el} as the input. For the lateral motion the A and B matrices with states β, ϕ, p, r, δ_a and δ_r with inputs δ_a and δ_r are constructed and presented by equation 5.

$$\begin{bmatrix} \dot{V_T} \\ \dot{\alpha} \\ \dot{\theta} \\ \dot{q} \end{bmatrix} = \begin{bmatrix} -0.0113 & 5.3133 & -32.1700 & -1.1275 \\ -0.0002 & -0.4577 & -0.0000 & 0.9627 \\ 0 & 0 & 0 & 1.0000 \\ -0.0000 & -1.8487 & 0 & -0.6361 \end{bmatrix} \begin{bmatrix} V_T \\ \alpha \\ \theta \\ q \end{bmatrix} + \begin{bmatrix} 0.0514 \\ -0.0010 \\ 0 \\ -0.0974 \end{bmatrix} \begin{bmatrix} \delta_{el} \end{bmatrix} \tag{4}$$

$$\begin{bmatrix} \dot{\beta} \\ \dot{\phi} \\ \dot{p} \\ \dot{r} \end{bmatrix} = \begin{bmatrix} -0.2846 & 0.0536 & 0.0355 & -0.9937 \\ 0 & 0 & 1.0000 & 0.0359 \\ -32.1134 & 0 & -3.2523 & 0.5810 \\ 9.9972 & 0 & -0.0203 & -0.4405 \end{bmatrix} \begin{bmatrix} \beta \\ \phi \\ p \\ r \end{bmatrix} + \begin{bmatrix} 0.0002 & 0.0007 \\ 0 & 0 \\ -0.7611 & 0.1153 \\ -0.0449 & -0.0789 \end{bmatrix} \begin{bmatrix} \delta_r \\ \delta_a \end{bmatrix} \tag{5}$$

The obtained LTI models are without actuator dynamics. In order to use these, the applicability needs to be verified. This can be done by calculating both models with and without actuator dynamics in series and check if Matlab computes the same results. The actuator dynamics are shown in equation 6. The calculations of both models are shown in table 4. The results from table 4 shows both models have the same eigenvalues, therefore are the same LTI model.

$$H_{servo} = \frac{20.2}{s + 20.2} \tag{6}$$

Longitudinal system dynamics	**Longitudinal system dynamics + servo**	**Lateral system dynamics**	**Lateral system dynamics + servo**
-0.548 - 1.33i	-0.548 - 1.33i	-0.251 - 2.63i	-0.251 - 2.63i
-0.548 + 1.33i	-0.548 + 1.33i	-0.251 + 2.63i	-0.251 + 2.63i
-0.00454 - 0.0711i	-0.00454 - 0.0711i	-1.44	-1.44
-0.00454 + 0.0711i	-0.00454 + 0.0711i	-0.00837	-0.00837
-20.2	-20.2	-20.2	-20.2
		-20.2	-20.2

Table 4: Eigenvalues for the longitudinal/lateral system dynamics with(out) servo

2.2 Analysis of eigenmotions and their characteristics

The aircraft has a total of 5 eigenmotions which can be divided in periodic and aperiodic eignmotions. The behavior of each eigenmotion will be analysed on the following properties:

- Natural frequency ω_n
- Damping ratio ζ
- Period P
- Time to half amplitude $T_{1/2}$
- Time constant τ

2.2.1 Analysis of periodic eigenmotions

The analysis of the F16-model resulted in 3 distinct complex poles, each corresponding to a specific eigenmode. These pairs are shown in table 5. Two eigenmodes belong to the longitudinal eigenmodes (short period and phugoid), the other one belongs to the lateral eigenmode. To determine which pole pair belongs to which eigenmode, the characteristics of each eigenmode must be known. The short period is a fast damping eigenmode and corresponds to a high damping ratio ζ and a more negative real part in the eigenvalue. The phugoid is a slowly damping eigenmode, which corresponds to the low damping ratio ζ and a more positive negative real eigenvalue. The pole pairs for the short period and phugoid motion are shown in figure 5. For the dutch roll, which is a lateral eigenmotion, the pole pair is shown in figure 6.

Eigenmotion	**Type**	**Poles**	ω_n **[rad/s]**	ζ **[-]**	**P [s]**	$T_{1/2}$ **[s]**	τ **[s]**
Short period	Symmetric	-0.548 ± 1.33i	1.4384	0.3810	4.368	1.26	-
Phugoid	Symmetric	-0.00454 ± 0.0712i	0.0713	0.0637	88.1	152.6	-
Dutch roll	Asymmetric	-0.251 ± 2.63i	2.65	0.0949	2.37	0.262	-

Table 5: Properties of the symmetric motions

2.2.2 Analysis of aperiodic eigenmotions

The analysis of the dynamics of the F16-model gives also results in poles which have no imaginary part. These are the aperiodic motions, that include the aperiodic roll and spiral mode, and are shown in table 6. In general, the aperiodic roll is a faster motion compared to the spiral motion. Therefore, the eigenmodes can be determined by the pole location. In table it can be seen that the eigenmotion which has a pole closer to the imaginary axis belongs to the spiral motion.

Eigenmotion	**Type**	**Poles**	ω_n **[rad/s]**	ζ **[-]**	**P [s]**	$T_{1/2}$ **[s]**	τ **[s]**
Aperiodic roll	Asymmetric	-1.44	1.44	-	-	0.48	0.692
Spiral motion	Asymmetric	-0.00838	0.00838	-	-	86.6	119

Table 6: Properties of the asymmetric motions

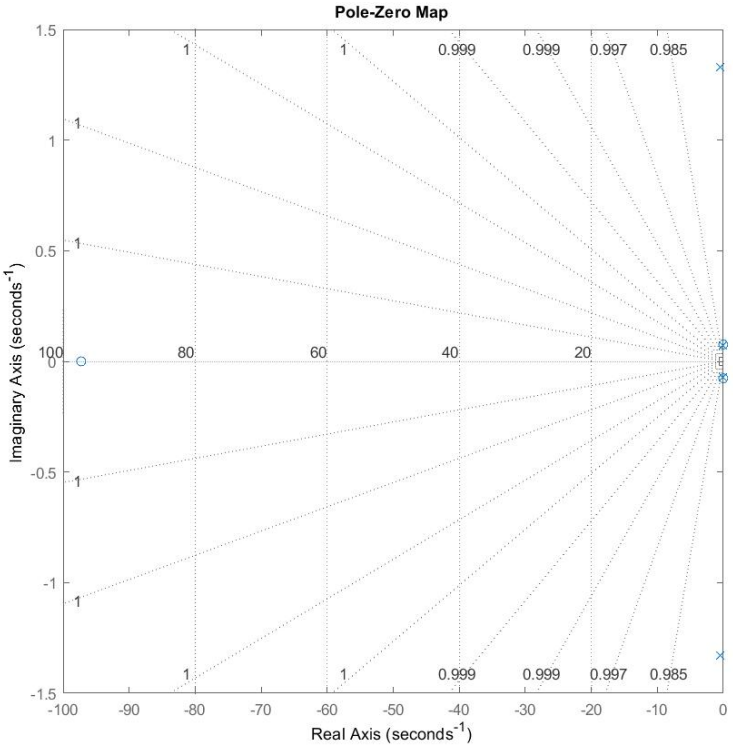

Figure 5: Pole zero map of the longitudinal system dynamics

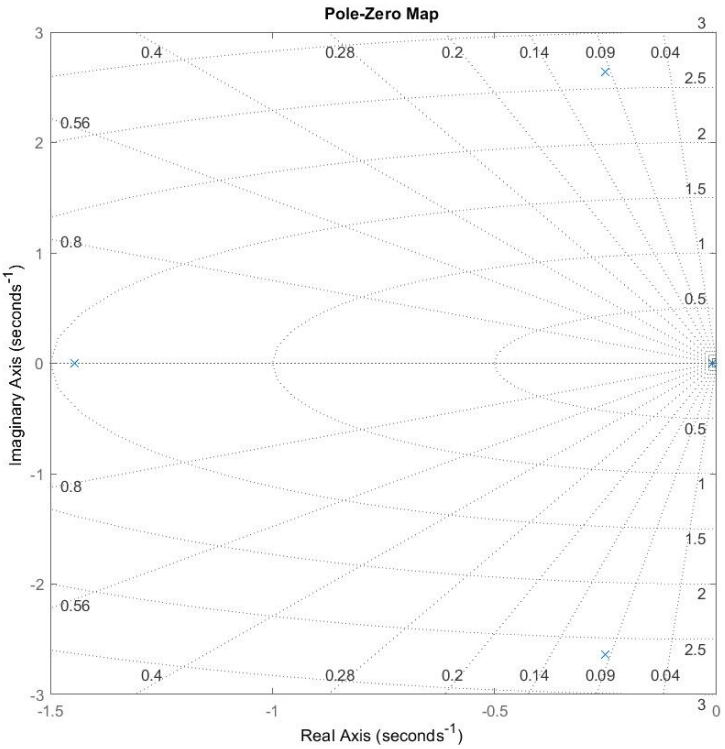

Figure 6: Pole zero map of the lateral system dynamics

2.3 Responses of the eigenmotions

The dynamic analysis results in five distinct eigenmotion. The time respones of these eigenmotions will be analysed by deflecting the elevator, aileron and rudder to visualize all the eigenmotions.

Figure 7 contains the longitudinal responses. The short period and phugoid are excited through the elevator deflections. On the first plot the step response of short period is shown and it acts as predicted. A quick change in the pitch rate followed by stabilizing behaviour due to the negative real part of the pole pairs. The phugoid is visualized through two plots, namely the velocity to time plot and angle of attack to time plot. This way of representing is interesting, because at the maximum of the angle of attack, the minimum of the velocity occurs, which is in line with theory. In both plots the second order under-damped behaviour is visible through its high period and slowly decreasing amplitudes over more oscillations.

The lateral motions are shown in figure 8, starting with the dutch roll. The dutch roll is excited by the rudder deflection, which intuitively excites a yawing motion (not shown) and also a rolling motion. As expected, the roll rate of the dutch roll is at a maximum when the yaw rate is at its minimum and visa versa. Again, the motion is a second order damped motion, which confirms the complex pole pairs. The period of table 5 is easily determined by the use of the plots.

The aperiodic roll and spiral motions are excited through a 5 degree aileron impulse (excited for 1 second). From the impulse response of the aperiodic roll it can be seen that this eigenvalue is very stable because it damps out very quickly. On the other hand the impulse response of the spiral motion which is indeed more slow returned to its original position. This makes the first order behaviour of both motions visible.

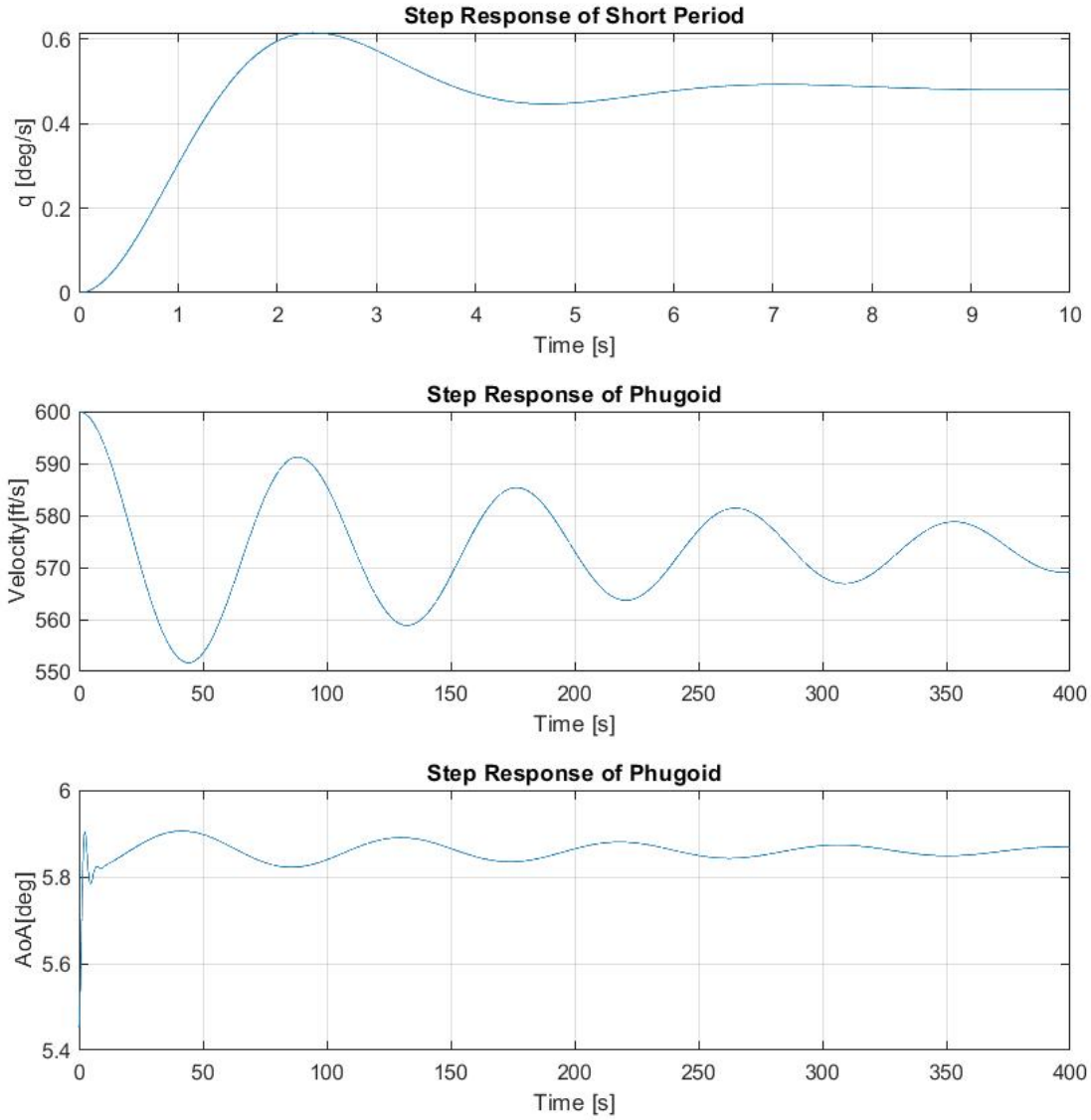

Figure 7: Longitudinal step-responses

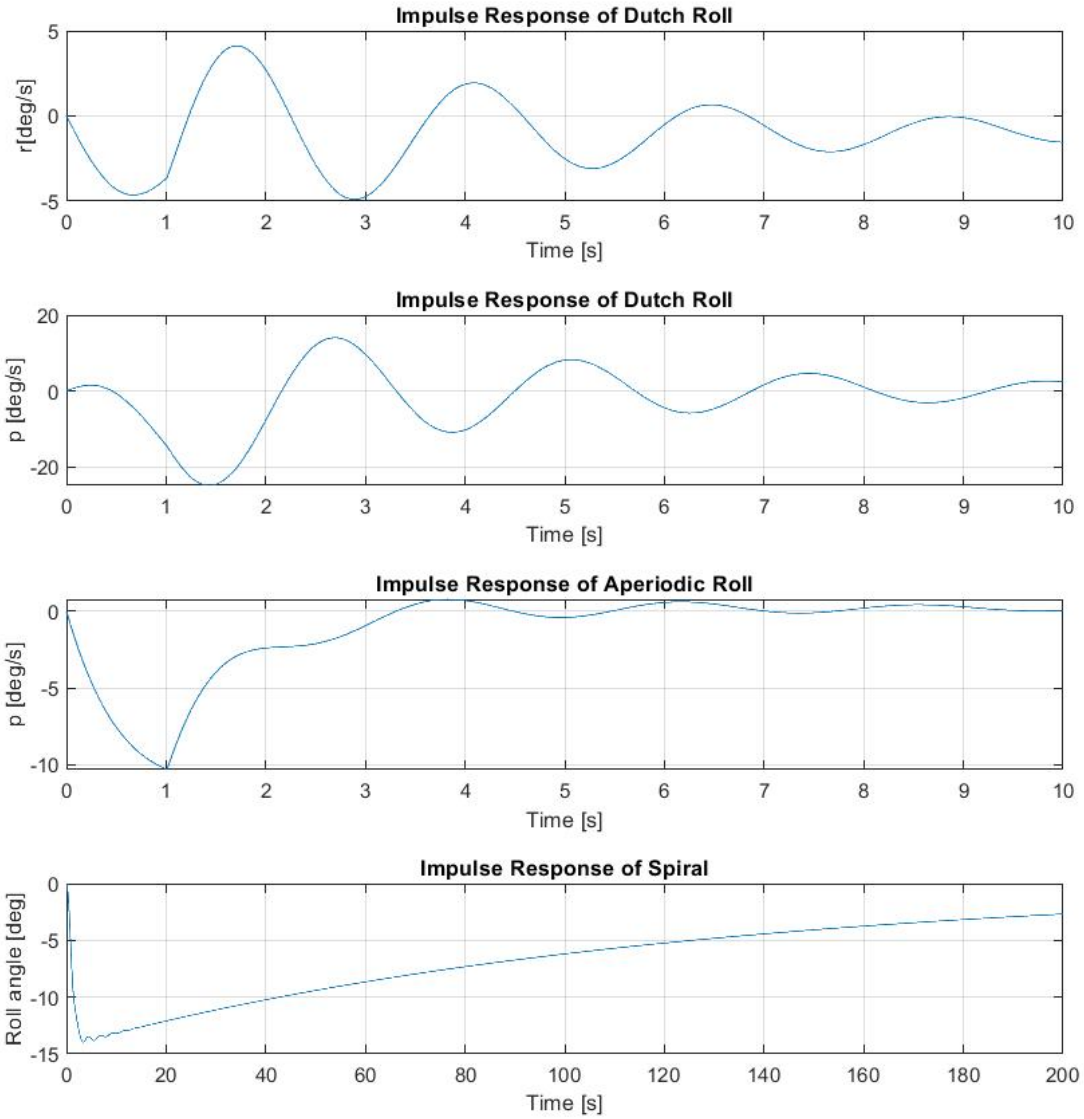

Figure 8: Lateral impulse-responses

3 Design of a Pitch Rate Command System

In this section the Control Anticipation Parameter (CAP) criterion and the Gibson criterion are used to design the Pitch Rate Command System of the F16 model. By using the 2 state reduced model, a feedback gain matrix and a lead-lag filter a pitch rate command system will be designed. In order to improve the steady state performance a gain is added. Figure 9 shows a schematic view of the the final design of the pitch rate command system. At last, this design has to be validated with the CAP and Gibson criteria.

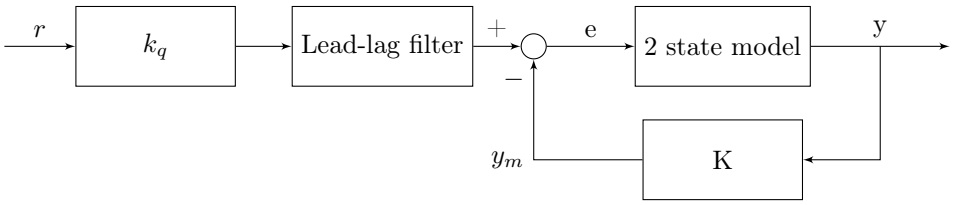

Figure 9: Block diagram of the pitch rate command system

3.1 Reducing the Short Period Model

From the 4 state longitudinal matrix without actuator dynamics shown in equation 4 from previous chapter the 2 state reduced model for the short period dynamics can be derived. This model only involves two states which are the angle of attack α and the pitch rate q. However, with this reduction some assumptions are made:

- The airspeed V_t remains constant so deviations of $V_{trim} = 0$
- Initial level flight conditions is assumed which means $\gamma_0 = 0$ and $C_{x0} = 0$

These assumptions allow for changes in 4 which will result in the desired simplified model which is used to analyse the short period dynamics. Because deviations of $V_{trim} = 0$ the first column can be eliminated. Also, this means that V remains constant and therefore the X_B axis force equilibrium is static. This enables to also eliminate the first row. Furthermore, In the third column of the A matrix all entries except the top one, which we eliminated, are 0 and we can eliminate this column. Finally, in the system we have left $\dot{\theta}$ is equal to the pitch rate q which enables for elimination of this row. With these eliminations the 2 state model we obtain is shown in formula 7 and 8, the C and D matrix are constructed such that angle of attack α and the pitch rate q are the outputs.

$$\begin{bmatrix} \dot{\alpha} \\ \dot{q} \end{bmatrix} = \begin{bmatrix} -0.4577 & 0.9627 \\ -1.8487 & -0.6361 \end{bmatrix} \begin{bmatrix} \alpha \\ q \end{bmatrix} + \begin{bmatrix} -0.0010 \\ -0.0974 \end{bmatrix} \delta_e \tag{7}$$

$$\begin{bmatrix} \alpha \\ q \end{bmatrix} = \begin{bmatrix} 1 & 0 \\ 0 & 0 \end{bmatrix} \begin{bmatrix} \alpha \\ q \end{bmatrix} + \begin{bmatrix} 0 \\ 0 \end{bmatrix} \delta_e \tag{8}$$

To validate whether this simplification is acceptable the time response to a step input of the 4 state and the 2 state are shown in figure 10. The top plot shows the time response in the first five seconds and the lower plot shows the time response over 30 seconds. It can be clearly seen that the difference of step input responses is negligible in the short term. After 5 seconds the time responses are starting to show a considerable difference which is the result of the phugoid motion. The phugoid motion is a significantly slower eigenmotion compared to the short period motion and therefore the short period is completely damped before the phugoid has completed one cycle. With this fact the simplification of the 4 state model to the 2 state model is considered acceptable because the difference during the short period motion is negligible.

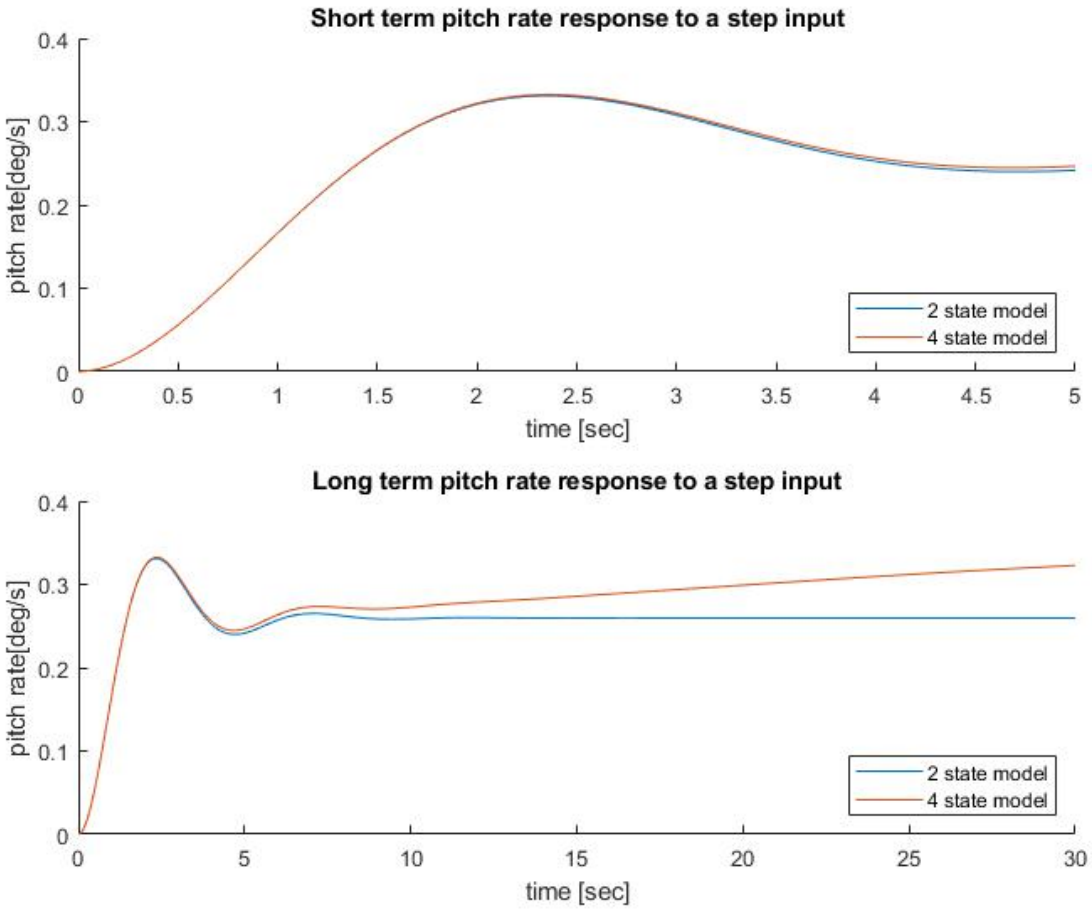

Figure 10: Step response of the 2 and 4 state model

3.2 Designing the Controller

The basis in the design of the Pitch rate Command system will be the 2 state derived model from previous section. it does not yet behave like desired by the CAP and Gibson criteria and therefore will have to be tuned. Requirements by CAP and Gibson are given in terms of natural frequency $\omega_{n_{sp}}$, time constant T_{θ_2} and damping ratio ζ which are defined respectively in equations 9, 10 and 11. These terms are only dependent on the velocity, in this case is 600 ft/s, and are used to construct the desired transfer function for the controller which is shown in equation 12. From this desired transfer function it is possible to calculate the desired poles by setting the denominator equal to zero which is done in equation 13. Note that the desired poles are not influenced by gain K_q.

$$\omega_{n_{sp}} = 0.03V = 0.03 \cdot 600 \cdot 0.3408 = 5.4863 \tag{9}$$

$$T_{\theta_2} = \frac{1}{0.75\omega_{n_{sp}}} = \frac{1}{0.75 \cdot 18} = 0.243 \tag{10}$$

$$\zeta = 0.5 \tag{11}$$

$$\left(\frac{q(s)}{\delta_e(s)}\right)_{desired} = \frac{k_q(1 + T_{\theta_2}s)}{s^2 + 2\zeta\omega_{n_{sp}}s + \omega_{n_{sp}}^2} = \frac{k_q(1 + 0.243s)}{s^2 + 5.4863s + 30.099} \tag{12}$$

$$P_{1,2_{desired}} = -\zeta\omega_{n_{sp}} \pm \omega_{n_{sp}}\sqrt{1 - \zeta}j = -2.7432 \pm 4.7514j \tag{13}$$

In order to obtain the desired poles a feedback matrix K is added to the 2 state model. This feedback matrix can easily be constructed using the pole placement design function in Matlab. For this system the function will give a matrix containing gains K_α and K_q as output which is given in equation 14.

$$K = [K_\alpha, K_q] = [-277.893, -42.2482] \tag{14}$$

In compliance with MIL-F-8785C the pitch rate command system has to be able to withstand severe vertical gusts of 4.572 m/s. Using this windgust the error of the angle of attack α can be calculated which is done in equation 15. Multiplying this error with the gain K_α results in the desired elevator deflection which is required to deal with the vertical gust, this is done in equation 16. The elevator of the F16 model can give a maximum deflection of $\pm 25°$ and therefore the desired elevator deflection to withstand the gusts is well within limits.

$$\alpha_{error} = arctan(\frac{V_{gust}}{V}) = arctan(\frac{4.572}{600}) = 0.025rad \tag{15}$$

$$\delta_{e_{demanded}} = K_\alpha \cdot \alpha_{error} = -277.893 \cdot 0.025 = -6.95° \tag{16}$$

With the current transfer function which is shown in equation 17 the denominator has the desired poles but the numerator is not yet equal to the desired numerator as shown in equation 12. In order to also change the numerator in a desired way a lead-lag filter will be added. Due to the denominator already being in the desired form the filter will be placed outside the feedback loop so it will not affect the denominator. The lead-lag filter will have the form as shown in equation 18. Multiplying the lead-lag filter with the current transfer function will cancel out the numerator of the current transfer function with the denominator of the filter. Also, the numerator of the total system will be taken from the filter. This will result in the transfer function as shown in equation 19.

$$(\frac{q(s)}{\delta_e(s)})_{current} = \frac{2.998(1.375s+1)}{s^2+5.486s+30.1} \tag{17}$$

$$H_{lead-lag}(s) = \frac{T_{\theta_2}s+1}{T_{\theta_{2_{current}}}s+1} = \frac{0.243s+1}{2.998(1.375s+1)} \tag{18}$$

$$\frac{q(s)}{\delta_e(s)} = \frac{0.243s+1}{s^2+5.486s+30.1} \tag{19}$$

At this point in the design the only thing which is different from the desired transfer function is the absence of the gain k_q. Similar to the lead-lag filter the gain will be placed outside the loop because it only has to affect the numerator of the transfer function. The gain will improve the steady state performance and can be found by analysing the step response using the final value theorem as done in equations 20 and 21.

$$Y(s) = U(s)H(s) = \frac{1}{s}\frac{k_q(0.243s+1)}{s^2+5.486s+30.1} \tag{20}$$

$$\lim_{t\to\infty} y(t) = \lim_{s\to 0}(sY(s)) = \lim_{s\to 0}\frac{k_q(0.243s+1)}{s^2+5.486s+30.1} = \frac{k_q}{30.1} = 1 \tag{21}$$

Setting the steady state response $\lim_{t\to\infty} y(t)$ equal to one will result in a $1°/s$ when the elevator is deflected 1 degree. In this case the gain k_q will be equal to 30.1. However, to make the aircraft react more or less sensitive to stick inputs equation 21 could be set equal to a different value and solving again for k_q. Substituting the gain into the transfer function will result in the final transfer function shown in equation 22.

$$(\frac{q(s)}{\delta_e(s)})_{final} = \frac{30.1(0.243s+1)}{s^2+5.486s+30.1} \tag{22}$$

3.3 CAP and Gibson criterion

The last step is to check whether the system complies with the CAP and Gibson criteria. These values used to validate model are defined as shown in equations 23 and 24 respectively.

$$CAP = \frac{\omega_{n_{sp}}^2 g T_{\theta_2}}{V} = 0.3923 \tag{23}$$

$$\frac{DB}{q_{ss}} = T_{\theta_2} - \frac{2\zeta}{\omega_{n_{sp}}} = 0.0608 \tag{24}$$

In figure 11 the allowable regions and the performance of the pitch rate command system is given. As shown in the figure the system has an level one performance in all three flight phase categories.

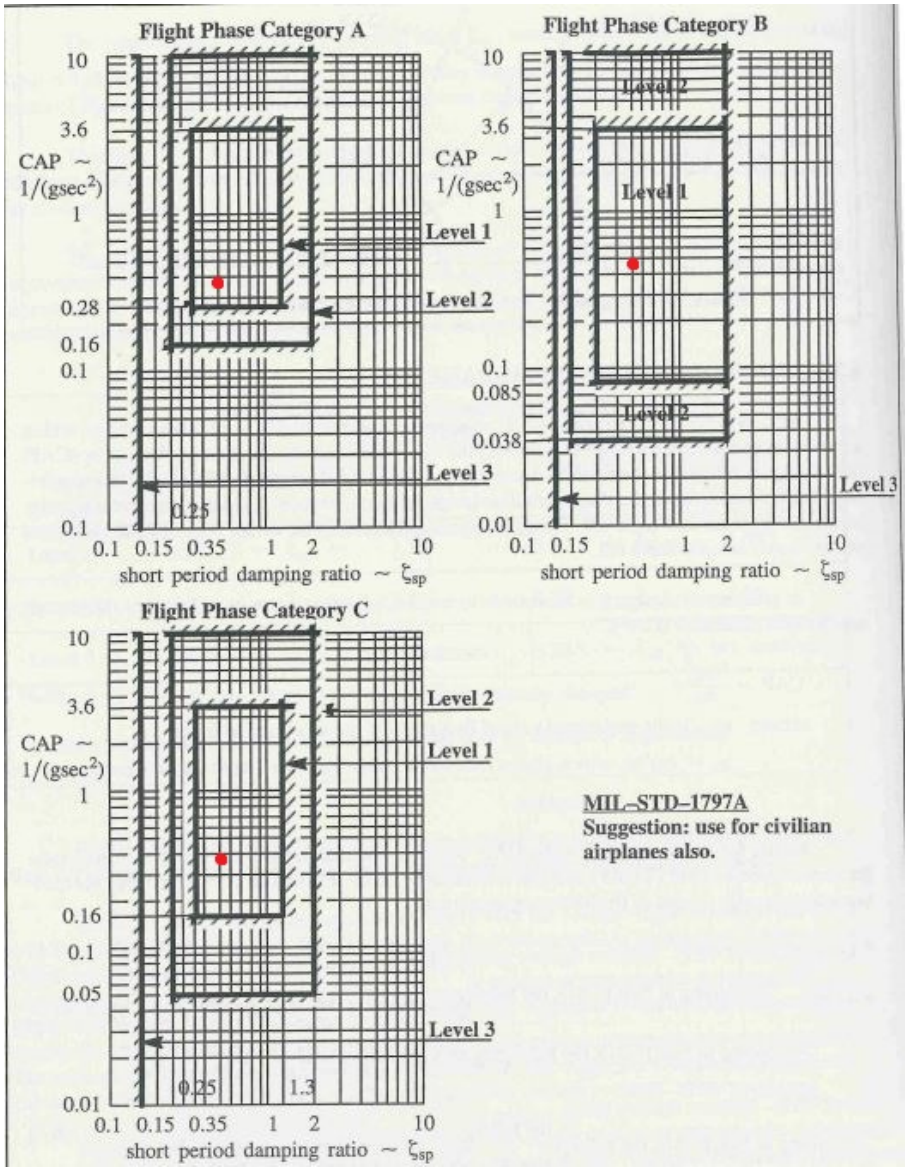

Figure 11: Control Anticipation Parameter

In order to determine whether the system lies within the limits of the Gibson criterion, the Gibson value and the maximum pitch rate over the steady state value of pitch rate $\frac{q_s}{q_m}$ are used. Figure 12 shows the time response of the pitch rate and pitch angle to a heaviside function as input, which is one between $t = 0$ and $t = 2$ and zero for all other t.

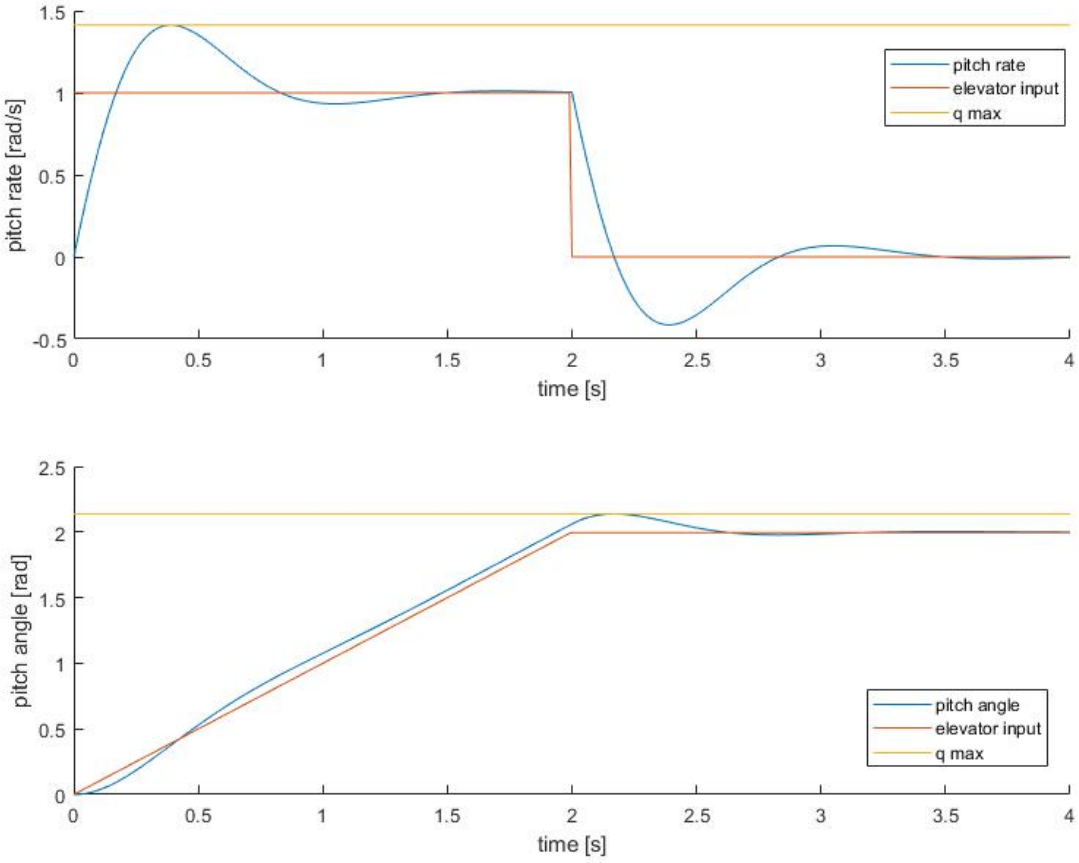

Figure 12: Time response to a heaviside input

From the pitch rate response it could be seen that the maximum pitch rate is equal to 1.4126. Because the steady state value of the pitch rate is equal to one the $\frac{q_s}{q_m}$=1.4126. From the pitch angle response the dropback or overshoot can be computed and divided by the steady state value which is done in equation 25. This value can be compared with the design value previously found with equation 24. In this particular case the system experiences a dropback which is desirable. In figure 13 it can be seen that the design point and the current value are both within the acceptable limits and is therefore in compliance with the Gibson criterion.

$$\frac{DB}{q_{ss}} = \frac{0.1382}{2} = 0.0305 \tag{25}$$

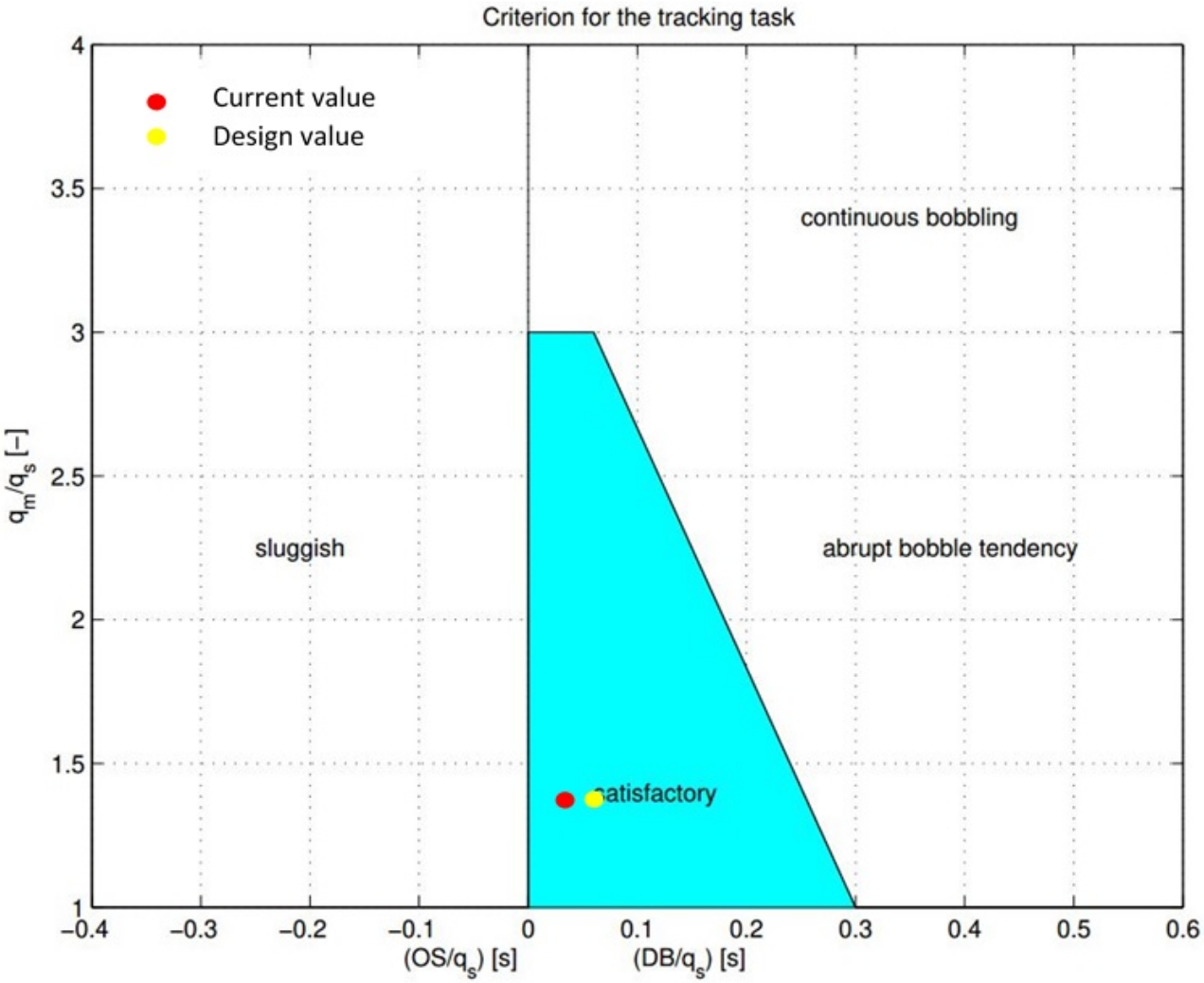

Figure 13: The Gibson criterion

4 Design of an Automatic Glideslope Following and Flare Controller

In this section the model set up and the simulation results of the Automatic Glideslope Following and the Flare controller are described. The system will be designed for a flight condition with an altitude of 5000 ft and a velocity of 300 ft/s. For both controllers an identical state space system is used which is shown in equation 26.

$$\begin{bmatrix} \dot{h} \\ \dot{\alpha} \\ \dot{\theta} \\ \dot{V}_t \\ \dot{q} \end{bmatrix} = \begin{bmatrix} 0 & 0 & -300.0 & 300.0 & 0 \\ 0.0001317 & -0.0291 & 2.13 & -32.17 & -2.895 \\ 3.154e-6 & -0.000697 & -0.5447 & 4.55e-13 & 0.9152 \\ 0 & 0 & 0 & 0 & 1.0 \\ -4.699e-21 & 1.038e-18 & 0.3303 & 0 & -0.8169 \end{bmatrix} \begin{bmatrix} h \\ \alpha \\ \theta \\ V_t \\ q \end{bmatrix} + \begin{bmatrix} 0 & 0 \\ -0.004534 & 0.001544 \\ -0.001116 & -9.493e-7 \\ 0 & 0 \\ -0.05702 & 0 \end{bmatrix} \begin{bmatrix} \delta_e \\ \delta_{th} \end{bmatrix} \tag{26}$$

Before the system is designed, an environment in which the landing procedure will be executed is created. After this, the modelling of the actuators which are used by the controllers are described. When this is defined, the design model of the controllers will be presented. Next, an analysis will be executed related to the states of the F16 over the entire operation. Conclusively, the performance of the controllers will be analysed by measuring the intended flight path tracking error.

4.1 Intended Flight path

Starting at an altitude of 5000 ft, the F-16 will intercept the glideslope after 10 seconds and tracks it until it will execute a flare manoeuvre and land at a runway with an altitude of 3000 ft. The total procedure will be executed with a velocity of 300 ft/s and the intended flight path without the flare manoeuvre is shown in figure 14.

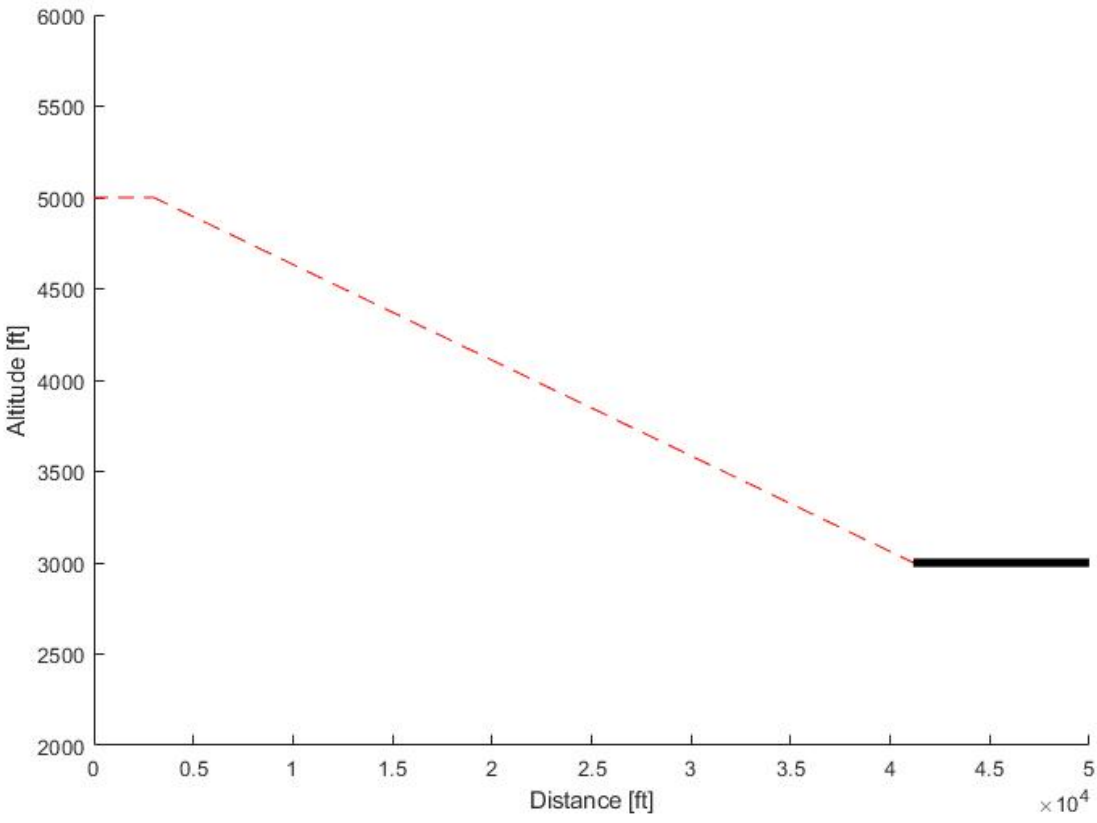

Figure 14: Intended flight path without the flare manoeuvre

4.2 Actuator models

The actuator models used for the elevator servo and thrust servo that are implemented in simulink as depicted in figure 15 and 16 and are defined in the following way:

- Elevator actuator : $\delta_e = \frac{20.0}{s+20.2} u_e$.
- Thrust actuator : $\delta_{th} = \frac{1}{s+1} u_{th}$.

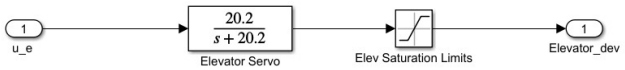

Figure 15: Elevator actuator in simulink

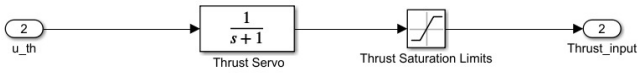

Figure 16: Thrust actuator in simulink

Both control inputs are subjected to saturation limits which are the defined by equation 27 in degrees and pounds respectively. The neutral position of the inputs are the trimmed values of the F16 at the given flight conditions.

$$\begin{aligned} -25 - \delta_{e_{trim}} \leq \delta_e \leq -25 - \delta_{e_{trim}} \\ 1000 - \delta_{th_{trim}} \leq \delta_{th} \leq 19000 - \delta_{th_{trim}} \end{aligned} \tag{27}$$

4.3 Model Structure

The architecture of the automatic glide slope following and flare controller is shown in figure 17. The design is at a first glance somewhat unclear, therefore in this chapter the design will be explained. For each subsystem the function, structure and critical aspects will be elaborated. The model can be divided in four subsystems which are the Roll Angle and Airspeed controller, the Glideslope Controller, the Mode Selector and the Flare Controller.

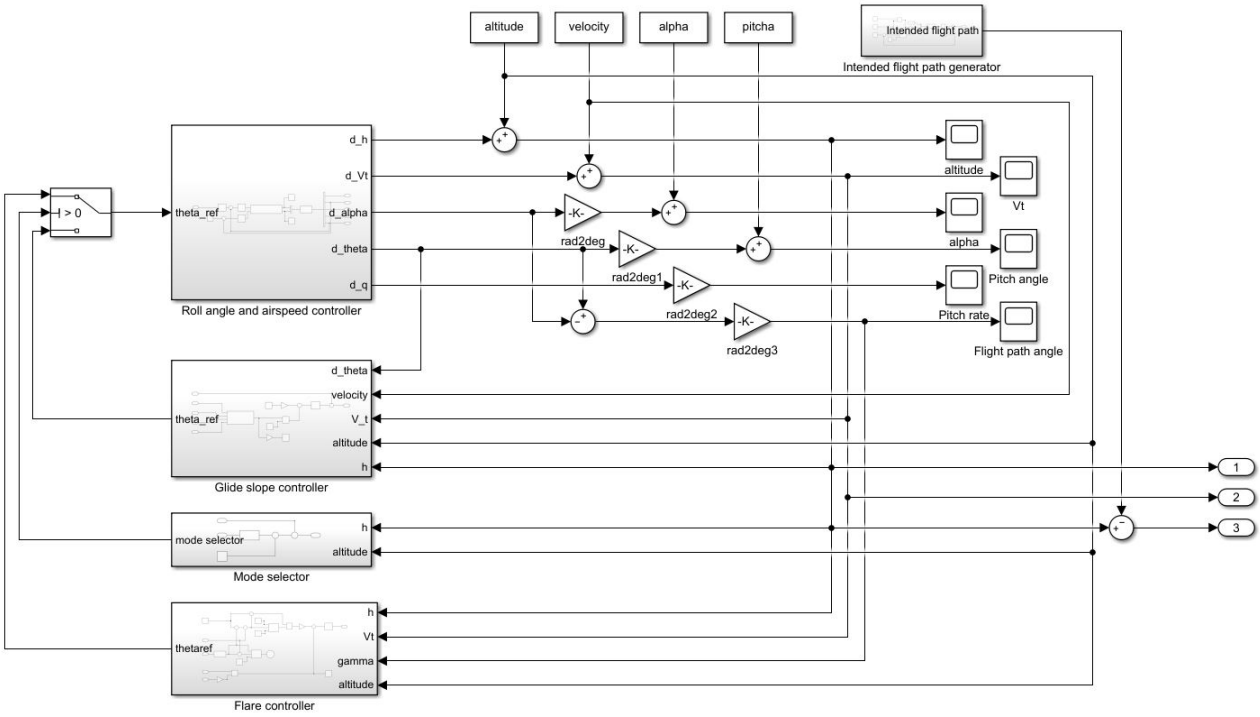

Figure 17: Design of the automatic glide slope following and flare controller

The initial altitude, velocity, angle of attack and pitch angle are added to the state space outputs to obtain the true values. The angle calculations of the states in the state space system is done in radians but for simplicity the angle of attack, pitch angle and flight path angle are converted to degrees for simplicity. In order to track the performance of the controlled flight path, a reference flight path is generated by the intended flight path generator block. Finally a switcher is used to automatically switch between the automatic glideslope following controller and the flare controller.

4.3.1 Inner Loops

In this section the inner loops are first tuned to match the desired pitch and speed performance. The model in simulink is shown in figure 18. With the state space, the dynamic responses of the system to the elevator and thrust inputs are simulated. The input of the model is a reference pitch angle (θ_r) which is then manipulated by a PID controller to create a reference pitch rate (q_r). The pitch angle feedback loop is not included in the Roll angle and airspeed controller simulink block, but can be seen in figure 17. This is the result of the way the flare controller is designed. The error pitch rate is then manipulated with a PID controller to generate an elevator actuator input. This signal is then fed to the actuators which is described in the previous subsection. The output of the actuators are elevator deflection(δ_e) and throttle setting (δ_{th}). These are used as inputs for the state space which is defined in equation 26. The C matrix is an identity matrix, to be able to produce all necessary outputs and finally the D matrix is a zero matrix.

The tuning process is started initially with the pitch rate to get the desired performance with a PID controller, thereafter the velocity controller is added. After that the tuning for the pitch angle is done by using a PID controller until the desired output is reached.

	q PID	**V PID**	**θ PID**
Proportional	-509.39	2000	3.36
Integral	-1672.89	50	1.4
Derivative	-25.6	1500	1

Table 7: PID values

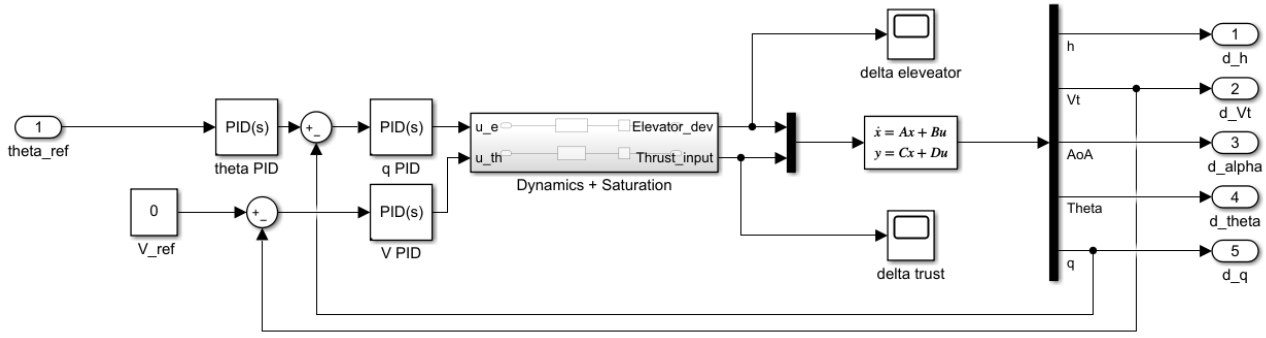

Figure 18: Pitch rate,Pitch angle and velocity controllers

4.3.2 Glideslope

In order to follow a glideslope path, the slant angle Γ has to be calculated. As shown in figure 19 the slant angle is defined as the angle between the three degrees glideslope path and the direct line between the glideslope transmitter and the glideslope antenna. Using the horizontal and vertical position of the aircraft (x_1, h_1) and the location of the glideslope transmitter (x_2, h_2) the slant angle can be calculated with equation 28.

$$\Gamma = 3 - tan^{-1}(\frac{h_1 - h_2}{x_2 - x_1}) \tag{28}$$

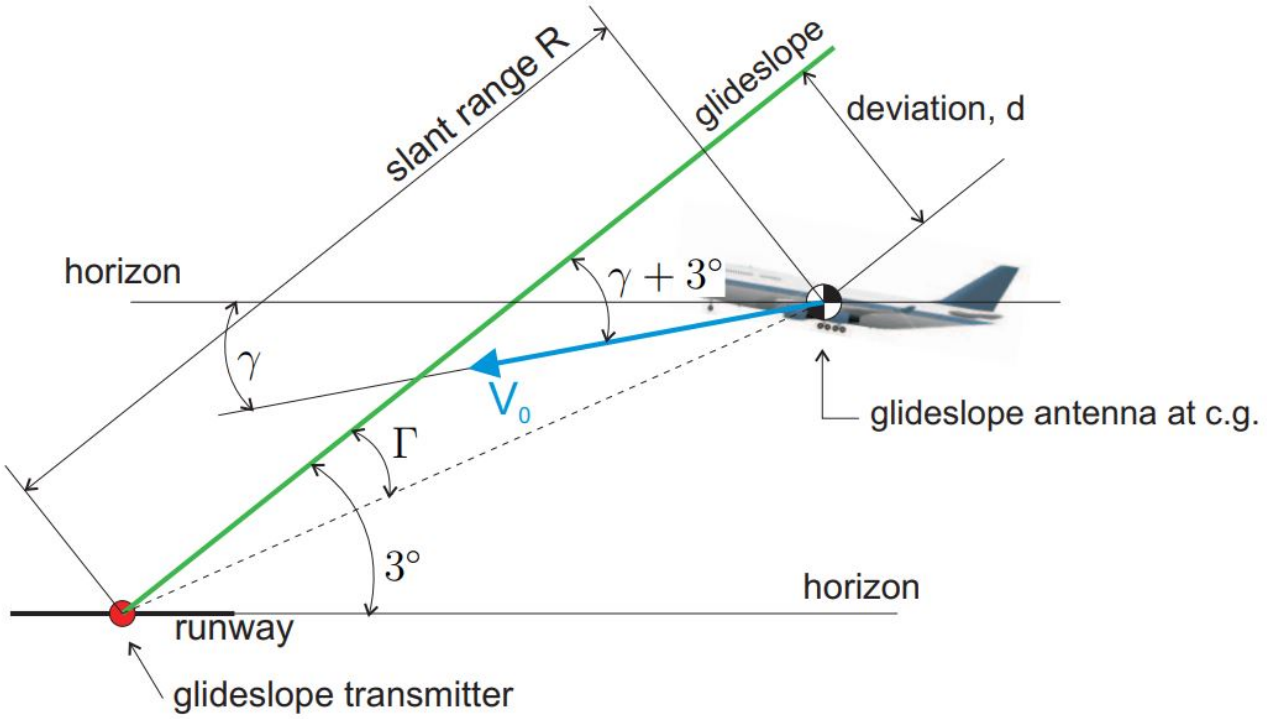

Figure 19: Schematic representation of approach situation

The slant angle calculator block of the glideslope controller uses the velocity and altitude at the beginning of the simulation to determine the location of the glideslope transmitter. The horizontal position of the aircraft can obtained by integrating the horizontal speed of the aircraft. However, the glideslope path has an angle of three degrees and therefore, the small angle approximation is valid. Because of this the horizontal position of the aircraft can be approximated by integrating V_t. The vertical position of the aircraft is equal to the altitude. The calculated slant angle is multiplied with a step input which has an initial value of zero and a final value of one to enforce that the glideslope will only be followed after ten seconds. This signal is compared to the reference slant angle of zero to obtain the slant angle error which is fed to the glideslope coupler which is a PID controller. From this controller a new reference pitch angle is computed. The simulink model depicted in figure 20 computes this calculation.

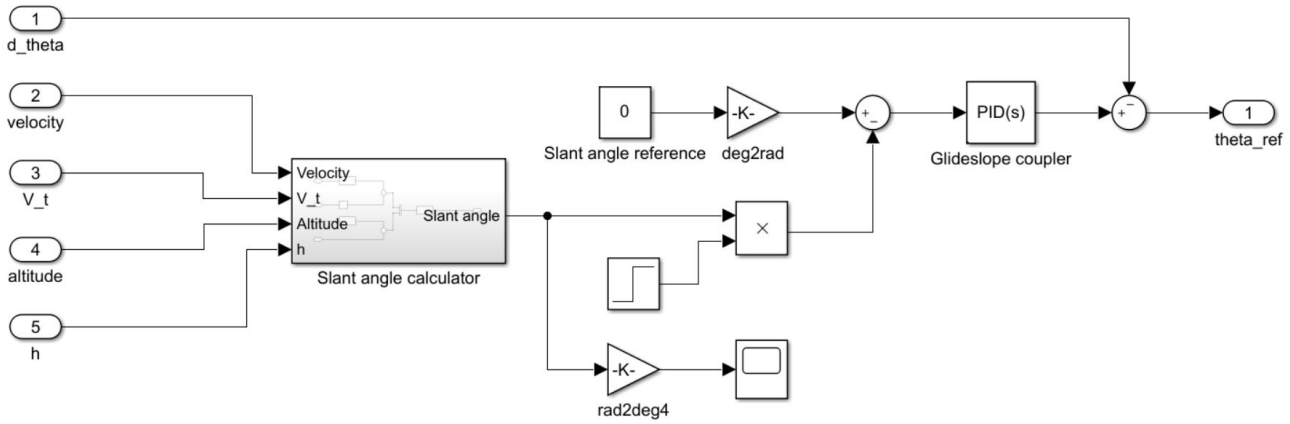

Figure 20: Glideslope controller

In order to obtain a satisfactory result the slant range feedback signal is designed to be fed back after 9.5 seconds, just before the glideslope interception. This minimises the lagging behind without increasing the altitude. As shown in figure 21 the flight path converges to the reference flight path again after the interception. This is enforced by the PID controller with the following controller parameters:

- Proportional: -55
- Integral: -5
- Derivative: 5

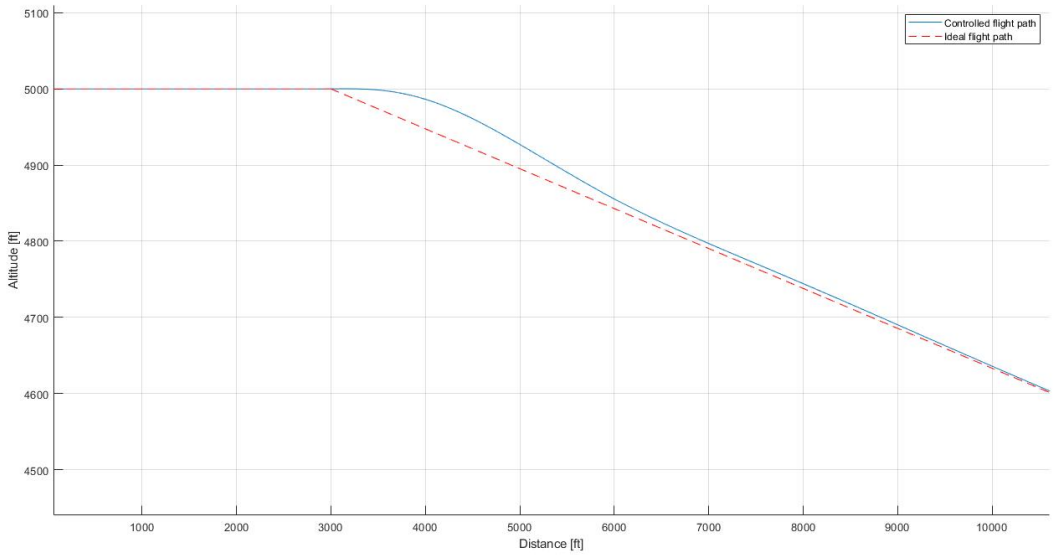

Figure 21: Interception of the glideslope

4.3.3 Mode Selector

During the flight envelope a change in controller must be initiated to follow the correct flight path. In this controller model there is one transition which is between the glide slope controller and the flare controller. As elaborated above the glide slope controller is initiated after a certain number of seconds due to a step input. This is also possible for the flare controller, but seems to be to simplistic due to the dynamic character of the combination of descending, controlling the glide slope error angle and the airspeed controller. Therefore, the flare controller is initiated at the flare height. So, the mode selector block shown in figure 22 initiates the transition from glide slope controller to flare controller.

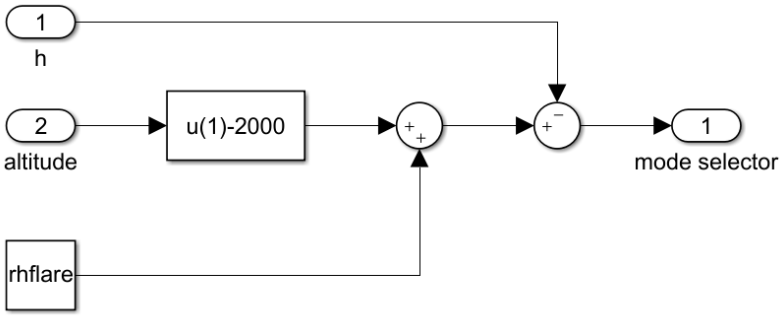

Figure 22: Mode selector block

4.3.4 Flare manoeuvre

The flare controller will adjust the controlled path to safely land on the airfield runway. It consists of some predetermined numbers which "should" make a correct flight path according to the theory. Figure 23 shows a schematic representation of the situation. The calculation of the flare height is based on the following assumptions:

- $V_t = 300 ft/s$
- $t = 2 * \tau$
- $X1 = 1000 ft$
- Flare path approximation: $h = h_{flare} * e^{-t/\tau}$.

The flare height computation is dependent on the airspeed of the F16. Due to the airspeed controller the airspeed stays within 302 feet/s and 299 feet/s. In addition, the P-controller has a very low gain in general and thus minor changes in altitude will not influence the model significantly. Therefore, it is valid to assume a constant velocity for calculating the flare height. The benefit of this assumption is a less complex system and less computation time. From these assumptions the calculated flare height is equal to 44 ft.
Consequently, the assumption of X1 is derived from the lecture slides example and will be validated through the simulation. X1 is the distance between the glide slope transmitter and the touchdown point.

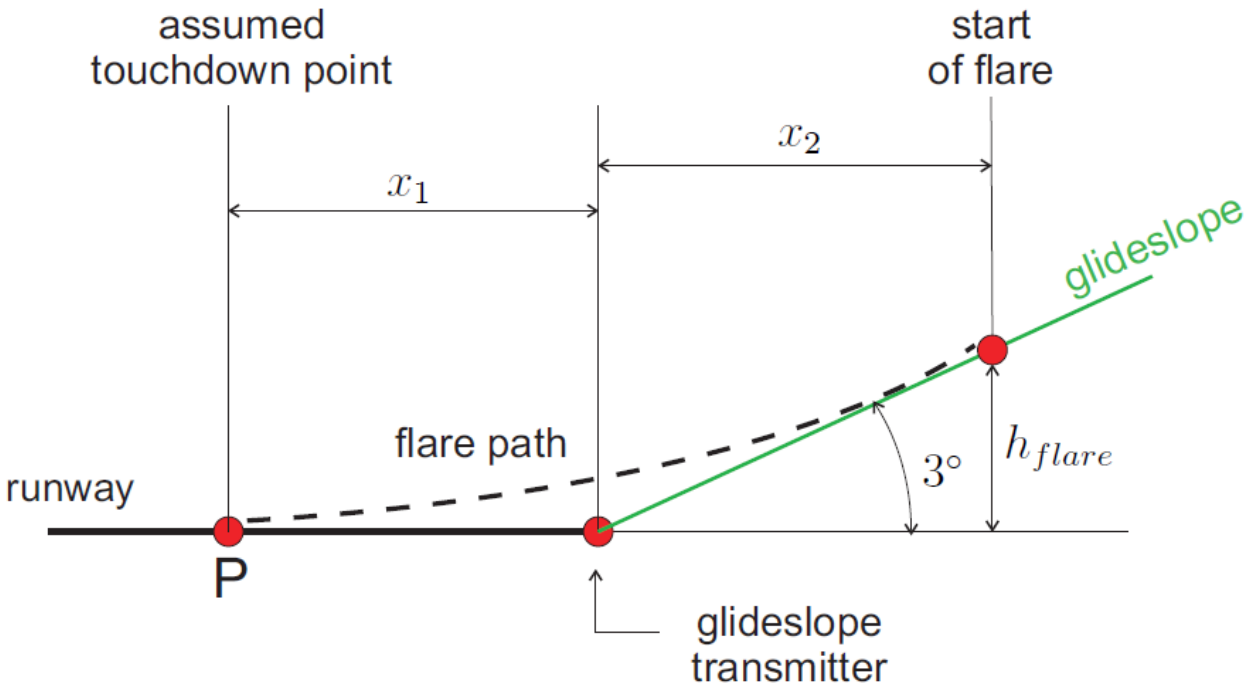

Figure 23: Flare path explanation

The flare controller becomes active once the flare height is reached. From that point the distance from the flare height to the actual height will be multiplied by a gain which result in a reference pitch angle. This value increases linearly with this difference and will be linked to roll angle and airspeed controller. As the F16 model touches the runway the simulation stops and the flare controller automatically becomes inactive. The architecture of the constructed flare controller is derived from the lecture example and is modelled in simulink as shown in figure 24.

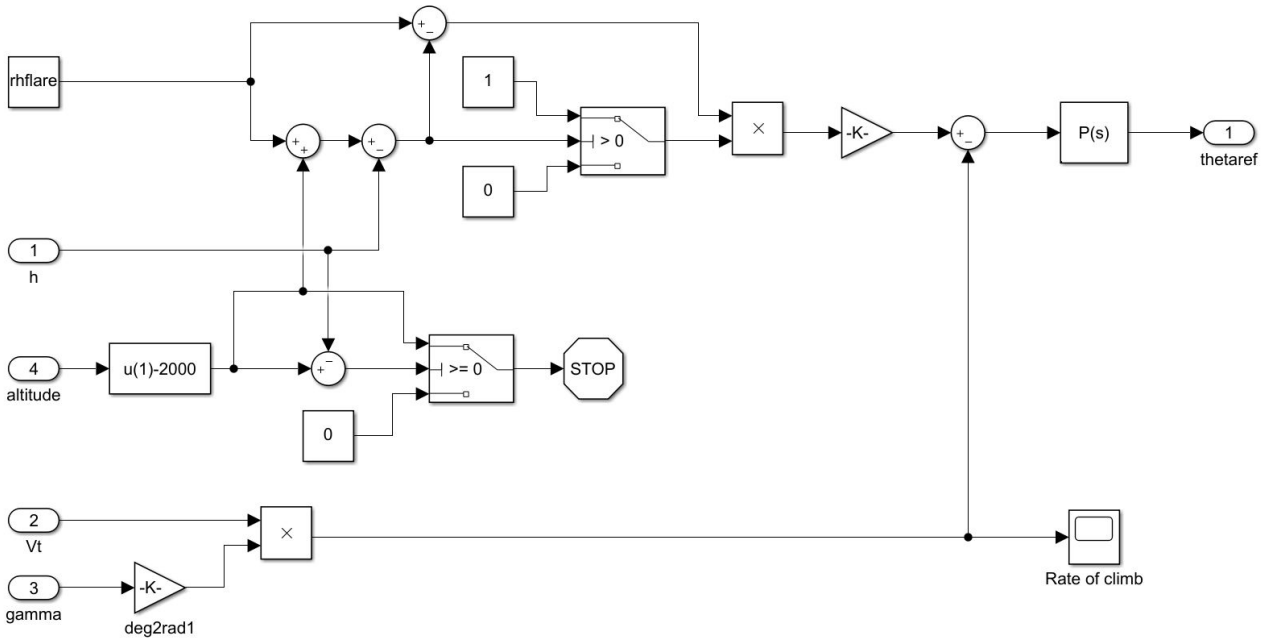

Figure 24: Flare controller

The vertical velocity during flight must be small for passenger comfort and to not exceed structural limits, but hard enough to avoid a "floating" aircraft. A floating aircraft is difficult to control and the touchdown point is not clearly determined. In conclusion, an acceptable vertical velocity directed to the runway is:

$$2ft/s \geq \dot{h} \geq 3ft/s$$

As a guideline for the controller the aim is to obtain a vertical velocity of 2,5 ft/s at touchdown. Initially, the inserted values in the flare controller does not result in an acceptable vertical velocity which is 150 ft/s when no controller is added. Therefore, this has to be tuned by a p-controller to correct for this undesirable error. After rerunning the simulation several times a proportional value of 0.00051045 does satisfy the requirements exactly. The vertical velocity over the entire flight envelope is shown in figure 25. At 134 seconds the flare is activated and the transient phase starts which ends at touchdown with a vertical velocity of 2.5 ft/s. The simulation shows that X1 and X2 are respectively 250 ft and 850 ft. Thus, the simulated X2 is only a quarter of the predetermined X1. An early conclusion can be derived from the fact that the predetermined values are based on a B747-200. The dynamics and controls are very different for a F16 and a B747-200 due to inertia and aerodynamics and so will be the flight path. As a result, the different dynamics which are typical for a F16 must be the reason for the shorter X1 and therefore a touchdown point which is closer to the glide slope transmitter is calculated prior to the simulations. The final controlled flight path during the flare manoeuvre is shown in figure 26.

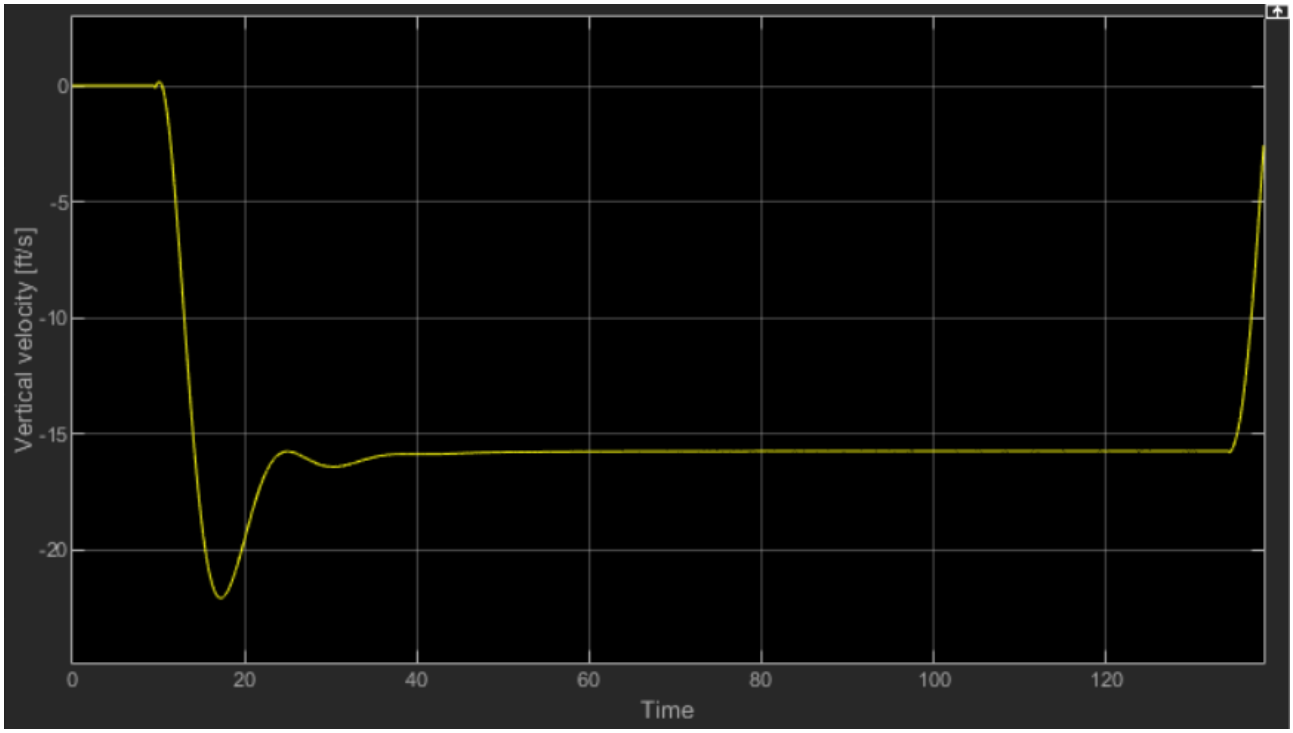

Figure 25: Vertical velocity during total flight

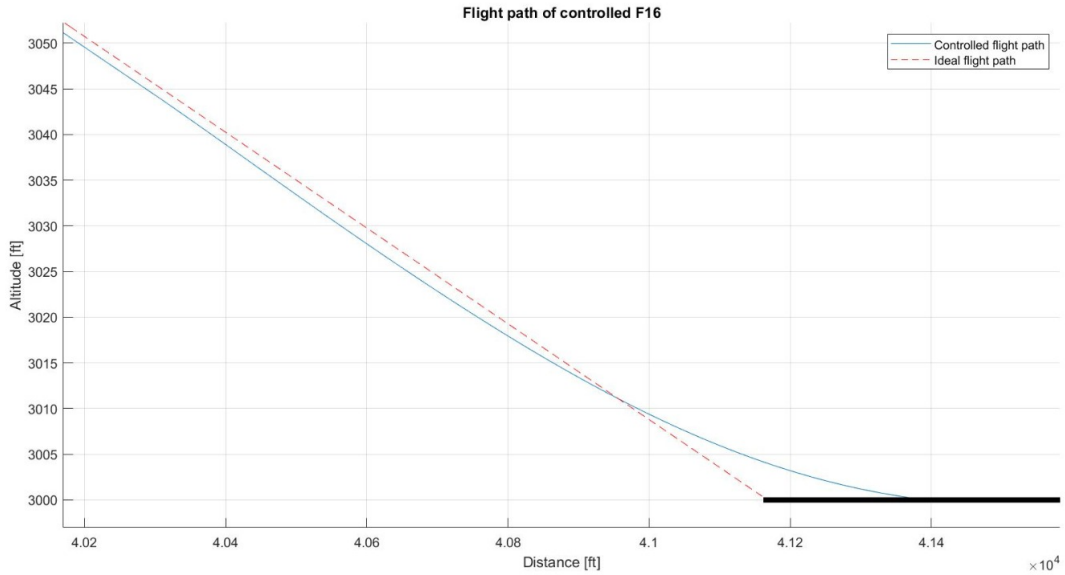

Figure 26: Flare manoeuvre

4.4 State analyses of the complete flight envelope

The pitch rate, pitch angle, flight path angle and elevator deflection are analysed to understand the glideslope interception and flare manoeuvres. All the prior mentioned states are depicted in figure 27, 28, 29 and 30. Because the glideslope controller will be initialised at 9.5 seconds the elevator will have a short negative followed by a short positive deflection which will decrease the pitch rate. This results in a decrease in pitch angle which will converge after some periods to a value for which the aircraft will follow the intended flight path of 3 degrees. As the flare is initiated a large elevator deflection will increase the pitch rate which will change the F16's attitude. Consequently, the pitch angle becomes larger to reduce the vertical velocity as expected.

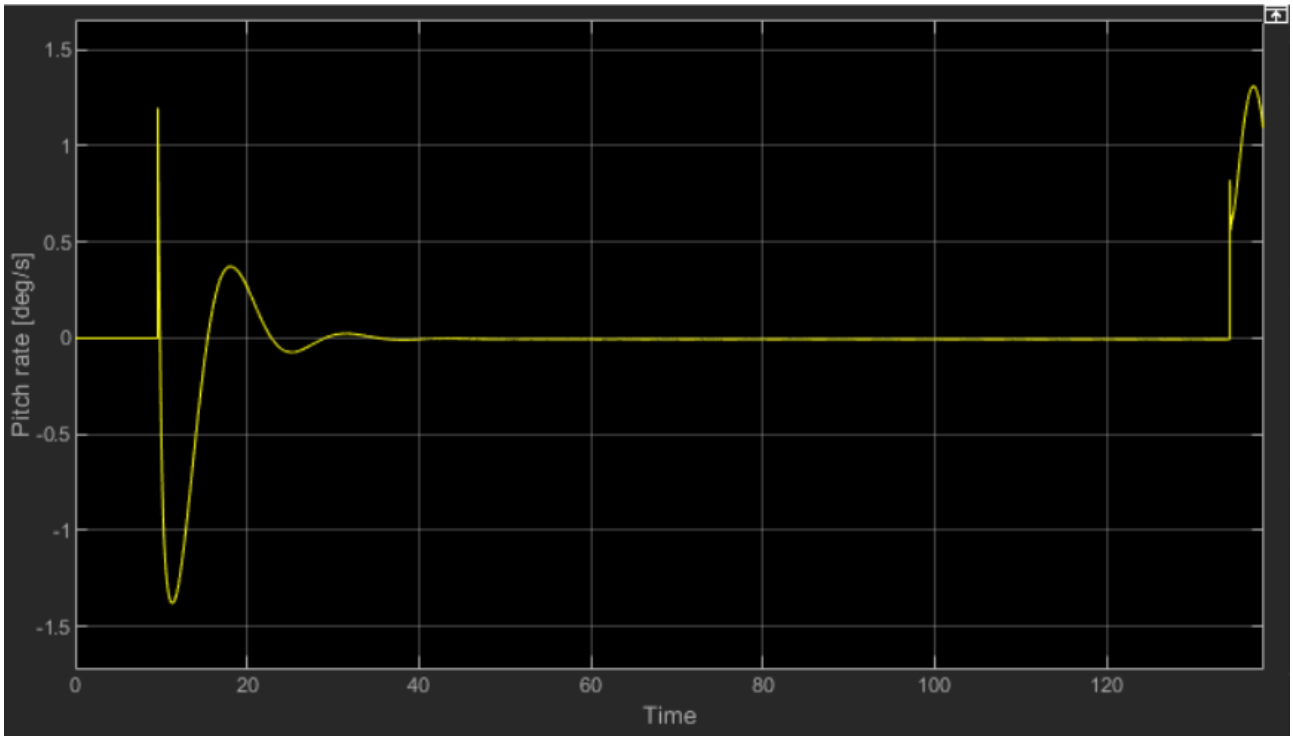

Figure 27: Pitch rate

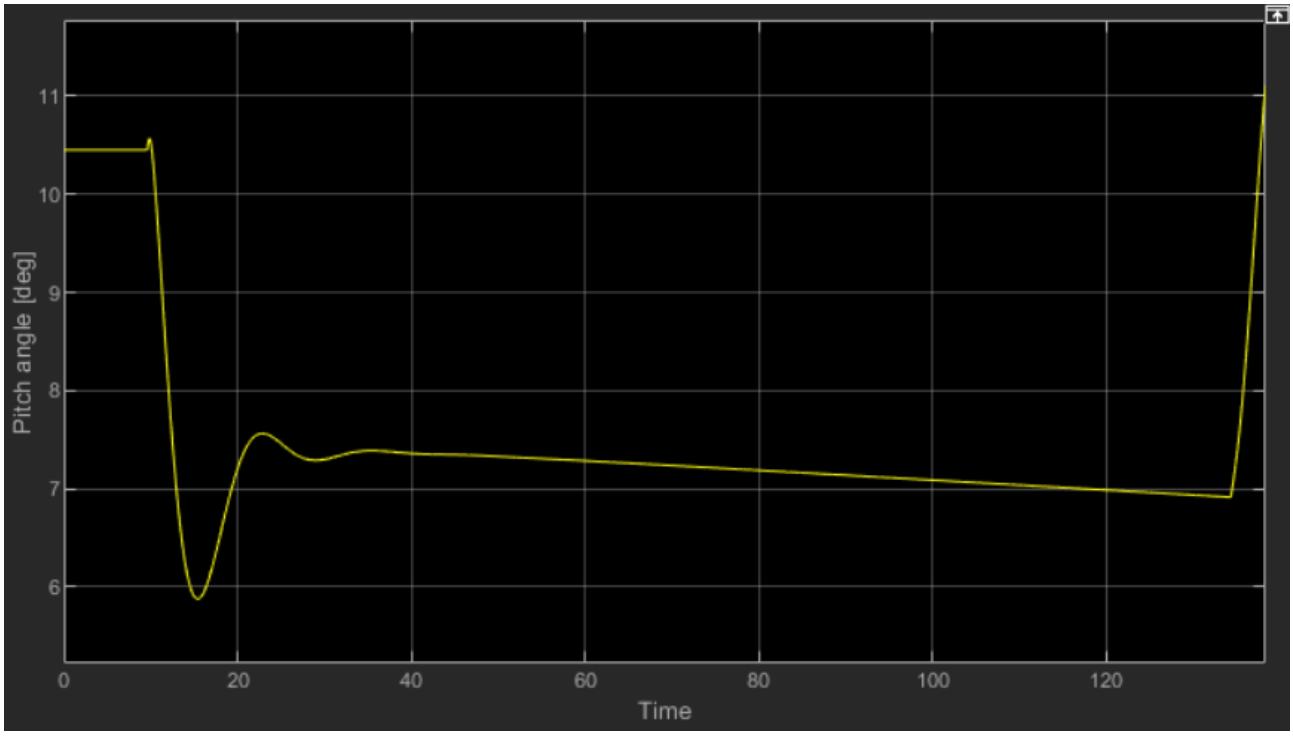

Figure 28: Pitch angle

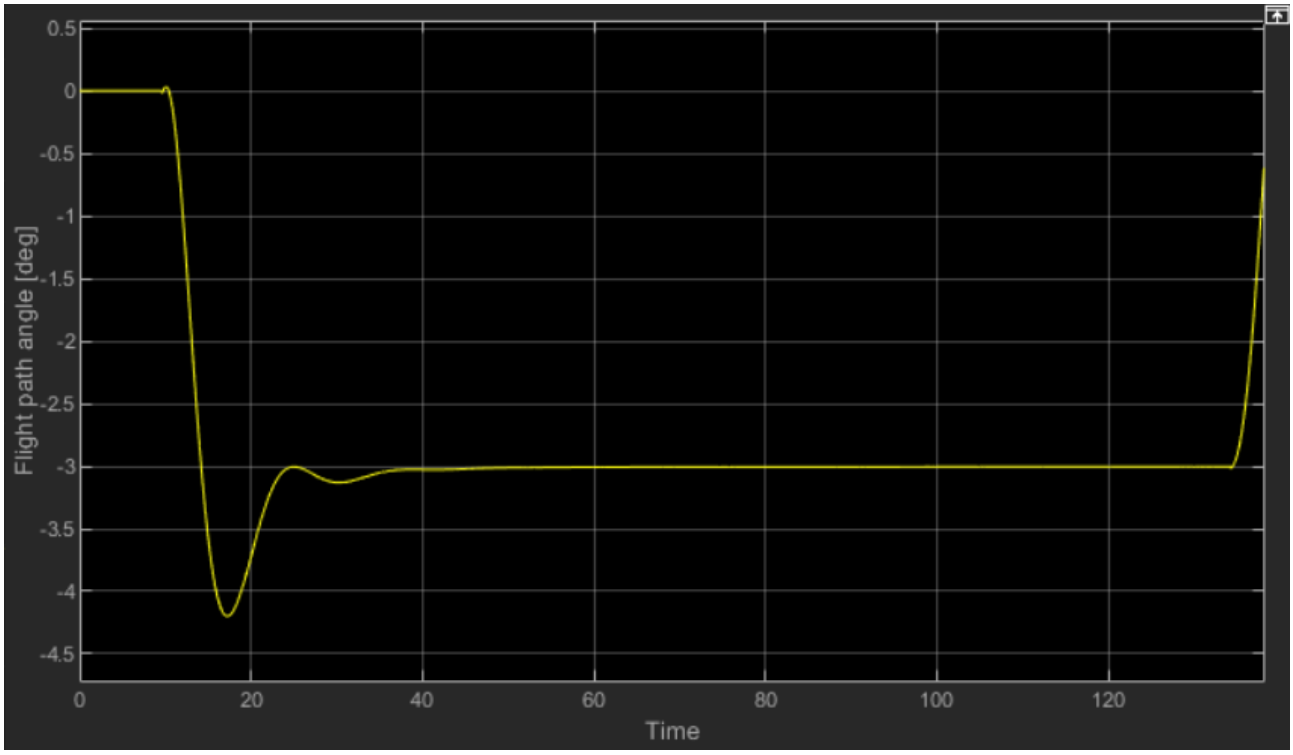

Figure 29: Flight path angle

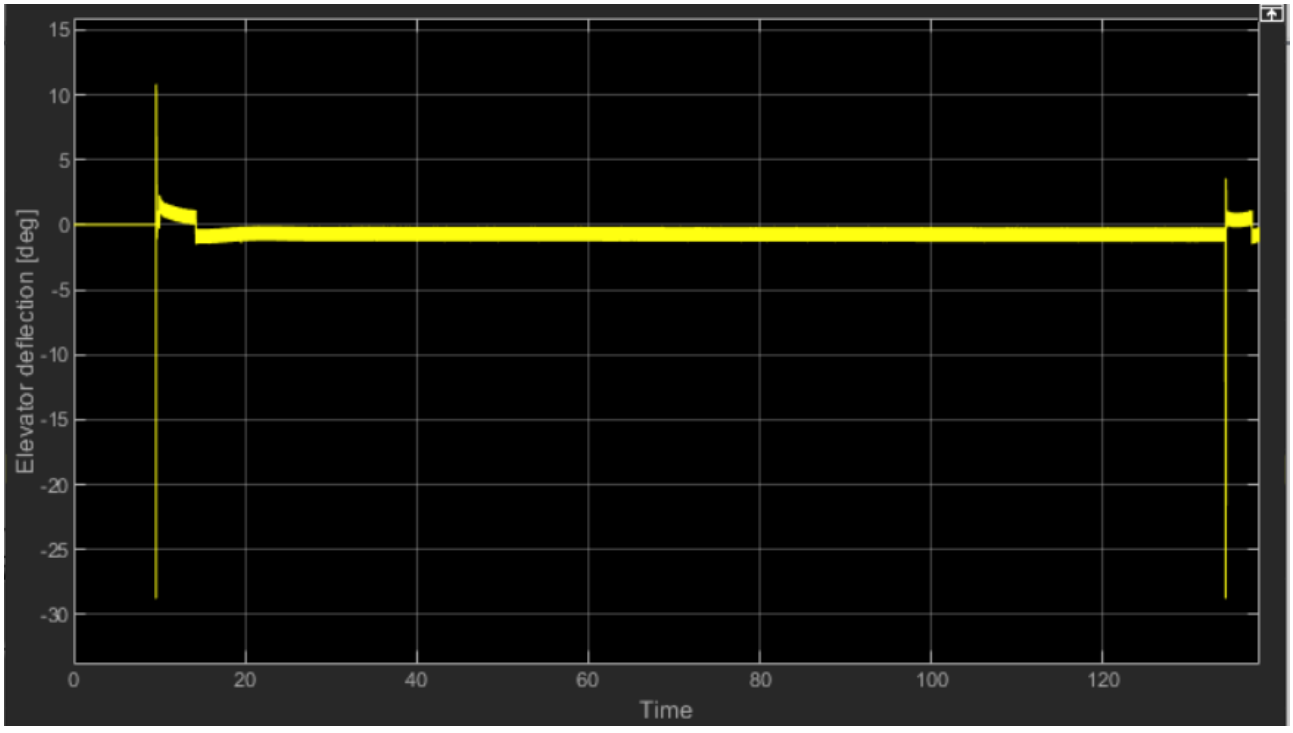

Figure 30: Elevator deflection

4.5 Tracking performance error

Figure 31 shows the difference between the intended flight path the actual path flown by the aircraft. In the first 10 seconds it can be seen that the error remains zero and quickly increases as the glideslope is intercepted. After this interception the error is corrected by a fight path angle which is bigger than 3 degrees. After some time it will converge back to an error of zero. However, it can be seen from the figure that the error slowly increases linearly over time. This neglectable error occurs due to the small angle approximation.

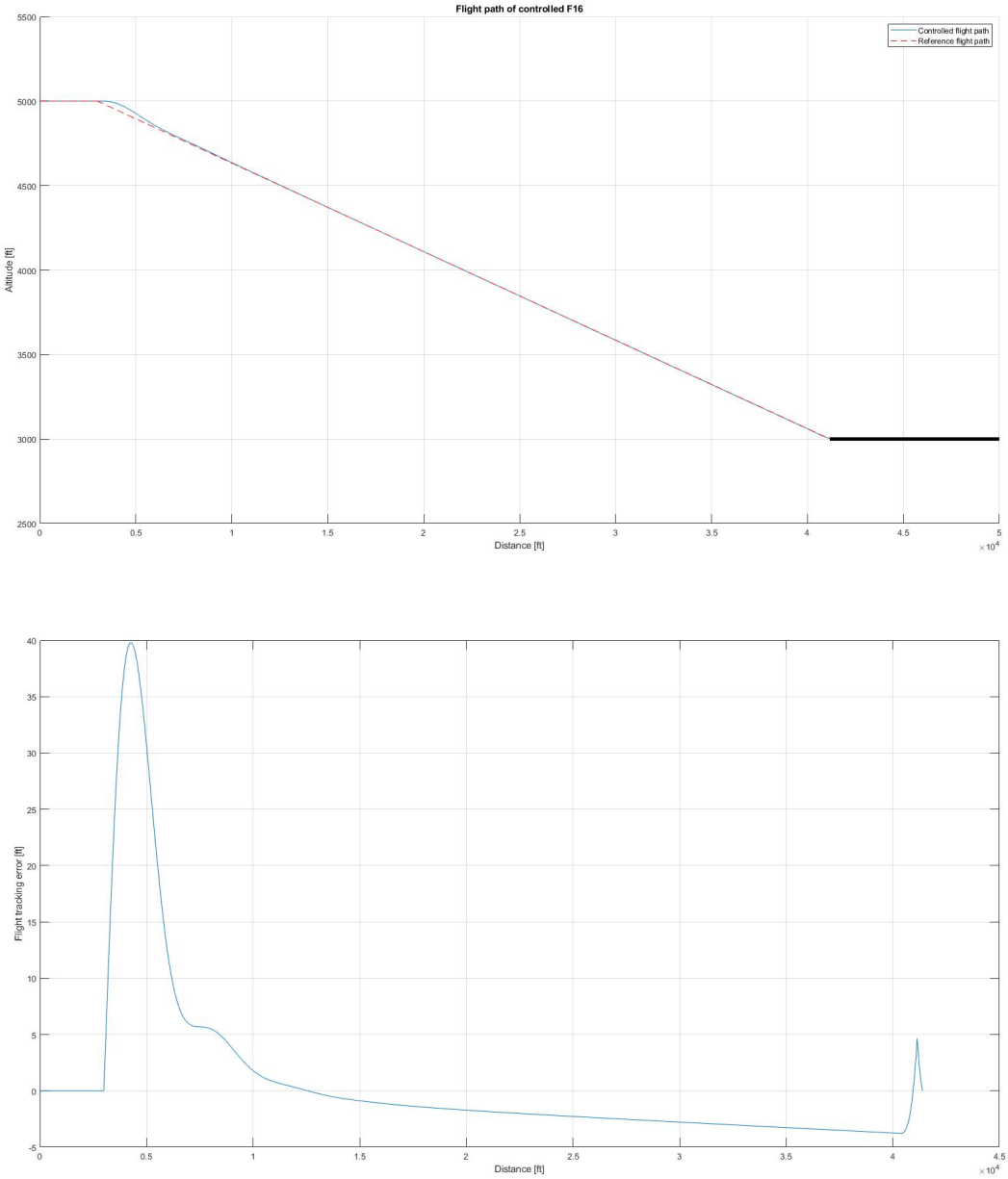

Figure 31: Tracking performance error

5 Conclusion

After the trim and liniearisation procedure of the high and low fidelity model, the accelerometer position is determined. This position was found along the X_b-axis close to $x_a = 5.9$ ft. With a reduced state space model of 4 states the an open loop analysis is carried out. It has been proven that this reduced model has the same eigenvalues as the original model with added actuators. All eigenmotion of the aircraft are linked to their corresponding poles and their behavioral properties are calculated. The time responses of all eigenmotions are evaluated. After this, the model is further reduced to only two states in order to design a pitch rate command system. It is proven that this 2 state model has a negligible difference in the pitch rate time response during the short period eigenmotion. For this state space model a lead-lag controller is designed in order to comply with the CAP and Gibson criteria. This is done successfully with a CAP value of 0.3923 and a Gibson dropback criterion value of 0.0305. Finally, the automatic glideslope following and flare controller are designed. Using a state space model which includes 5 states and 2 inputs a model for this controller is designed. As reference flight path is defined in order to be able to track the desired flight path. Actuator models with saturation limits are added to the inputs of the state space system. The total architecture of the controller is divided into 4 subsystems each with a specific function. In order to get more understanding in the manoeuvres during the entire flight envelope a state analysis is executed. The performance of the model is measured with the flight path error, vertical velocity at touchdown and touchdown distance after the glideslope transmitter. With a vertical velocity of 2.5 ft/s and a touchdown distance of 250 ft after the glideslope transmitter a satisfactory result is obtained.

References

[1] E. van Kampen. “Practical assignment AE4-301P: Exercise Automatic Flight Control System Design”. 2019.

[2] Richard S. Russel. “Non-linear F-16 Simulation using Simulink and Matlab”. 2003.

[3] Brian L. Stevens, Frank L. Lewis, and Eric N. Johnson. *Aircraft Control and Simulation*. Wiley-Blackwell, 2015.